Nanoscale

# Synthesis, growth mechanisms, and applications of palladium-based nanowires and other one-dimensional nanostructures



| | |
|---|---|
| Journal: | *Nanoscale* |
| Manuscript ID | NR-REV-07-2019-005835.R1 |
| Article Type: | Review Article |
| Date Submitted by the Author: | 09-Aug-2019 |
| Complete List of Authors: | kumar, Abhishek; University at Buffalo (SUNY), Department of Chemical and Biological Engineering<br>Mohammadi, Mohammad Moein; University at Buffalo (SUNY), Department of Chemical and Biological Engineering<br>Swihart, Mark T.; University at Buffalo (SUNY), Department of Chemical and Biological Engineering; |
| | |

ARTICLE

# Synthesis, growth mechanisms, and applications of palladium-based nanowires and other one-dimensional nanostructures

Received 00th January 20xx,
Accepted 00th January 20xx

DOI: 10.1039/x0xx00000x

Abhishek Kumar,[a] Mohammad Moein Mohammadi[a] and Mark T. Swihart*[a,b]

Palladium-based nanostructures have attracted the attention of researchers due to their useful catalytic properties and unique ability to form hydrides, which finds application in hydrogen storage and hydrogen detection. Palladium-based nanowires have some inherent advantages over other Pd nanomaterials, combining high surface-to-volume ratio with good thermal and electron transport properties, and exposing high-index crystal facets that can have enhanced catalytic activity. Over the past two decades, both synthesis methods and applications of 1D palladium nanostructures have advanced greatly. In this review, we start by discussing different types of 1D palladium nanostructures before moving on to the different synthesis approaches that can produce them. Next, we discuss factors including kinetic vs thermodynamic control of growth, oxidative etching, and surface passivation that affect palladium nanowire synthesis. We also review efforts to gain insight into growth mechanisms using different characterization tools. We discuss the effects of concentration of capping agents, reducing agents, metal halides, pH, and sacrificial oxidation on the growth of Pd-based nanowires in solution, from shape control, to yield, to aspect ratio. Various applications of palladium and palladium alloy nanowires are then discussed, including electrocatalysis, hydrogen storage, and sensing of hydrogen and other chemicals. We conclude with a summary and some perspectives on future research directions for this category of nanomaterials.

## Introduction

One-dimensional (1D) nanostructures are defined as those with two of their three dimensions below 100 nm, and one exceeding 100 nm. These 1D nanostructures are further classified into nanowires (NWs), nanorods (NRs), nanobelts, and nanotubes (NTs) based on their shape and aspect ratio, which is the ratio of their length to width or diameter. NWs (1D nanomaterials with length exceeding 100 nm) have attracted the attention of the scientific community because of electronic and plasmonic properties influenced by their small diameter, combined with a 1D structure that can provide enhanced electrical, mechanical, and thermal properties in thin films and nanocomposites. These properties have enabled the application of 1D nanostructures in several nanoscale devices such as flexible electronics, transparent conductors, optoelectronic devices, and chemical and biological sensing devices.[1,2]

*Abhishek Kumar obtained his B.Tech degree from Sardar Vallabhbhai National Institute of Technology, India. He is currently a doctoral candidate in Prof. Mark T. Swihart's group at the Chemical and Biological Engineering department of University at Buffalo (SUNY). His research focus is on palladium-based nanowire synthesis and applications.*

Palladium is a noble metal that plays a key role in many catalytic reactions, along with Pt. Apart from excellent catalytic activity towards the oxidation of small organic molecules and in dissociation of ethanol, methanol, and formic acid, palladium can play an important role in the hydrogen economy.[3] Palladium has a unique ability to dissociate hydrogen at its surface and store it in large volumetric quantity at ambient conditions in the form of palladium hydride ($PdH_x$).[4] This selective interaction of palladium with

*Mohammad Moein Mohammadi is a Ph.D. candidate in the Chemical and Biological Engineering Department, University at Buffalo (SUNY) under the supervision of Professor Mark T. Swihart since 2015. He received his Master's degree from Sharif University of Technology, Iran and his Bachelor's degree from Amirkabir University of Technology (Tehran Polytechnic), Iran. His current research interests include the design and synthesis of metal-containing nanomaterials via solution and gas phase (aerosol) techniques.*

[a] Department of Chemical and Biological Engineering, and [b] RENEW Institute, University at Buffalo, The State University of New York, Buffalo, NY 14260, USA.
* Corresponding author: swihart@bufalo.edu

hydrogen combined with the high surface to volume ratio and superior electrical conduction offered by 1D palladium nanowires enables application in hydrogen gas sensors.[5] However, the price of palladium has risen sharply in recent years, making it the costliest noble metal at $1438 per troy ounce, compared to $809 per troy ounce for Pt and $1336 per troy ounce of Au (Kitco Gold Index, June 10, 2019). This price surge is mostly due to the high demand for palladium-based catalysts in catalytic converters for automobiles. Despite this price surge, palladium is still an attractive electrocatalyst for direct alcohol fuel cells (DAFCs)[6] and formic acid oxidation reactions[7] where it has high high activity compared to commercial Pt/C catalysts. Relative to commercially-available Pd/C catalysts, palladium-based 1D nanostructures show enhanced activity towards electrochemical reactions owing to the presence of twin defects and exposed high-index facets.[8] High demand and rising prices of palladium have prompted researchers to either explore alternatives to palladium nanostructures or to reduce palladium usage while maintaining the same performance. Several studies have shown that alloying of palladium with transition metals at specific stoichiometric ratios can enhance particular properties relative to pure Pd.[3,9] Palladium alloy NWs are being explored for applications including electrocatalysis and hydrogen storage and sensing, where they can have improved performance relative to other palladium nanostructures due their expanded lattice and synergistic effect from changes in the electronic structure (*e.g.* position of the *d*-band center) of the bimetallic or trimetallic nanocrystals.[10,11]

Despite their advantages, the number of publications on 1D palladium nanostructures is limited. In the existing literature, the effects of dimensionality and morphology of palladium-based alloy NWs have not been fully explored. This review considers recent developments in the synthesis and applications of palladium and palladium alloy NWs. We begin with a brief description of 1D palladium nanostructures before moving on to the various methods used to achieve 1D growth. The next section discusses the growth mechanisms of palladium NWs and the mechanistic insight provided by various characterization tools. We then examine the chemistry behind solution phase synthesis of palladium-based NWs and discuss the effects of various reaction conditions and the concentrations of reducing agent and capping agents in solution phase synthesis. Different applications of palladium and palladium alloy NWs are discussed in the next section. Finally, the review ends with a brief discussion of future challenges and prospects of palladium and palladium-based alloy NWs.

*Mark T. Swihart is UB Distinguished Professor and Chair of Chemical and Biological Engineering at the University at Buffalo (SUNY). He earned his Ph.D. in chemical engineering from the University of Minnesota. He is a Fellow of the American Association for the Advancement of Science and the American Institute of Chemical Engineers (AIChE). The focus of his research is the synthesis and characterization, and applications of nanomaterials using both colloidal and aerosol*

## Types of 1D palladium nanostructures

One important factor used to classify 1D structures is their aspect ratio, which is the ratio of length to diameter. Generally, 1D palladium nanostructures with an aspect ratio less than 10 are called NRs and nanostructures with aspect ratio more than that are called NWs. Hollow NWs are called NTs. Based on the strategy used for NW synthesis, NWs can be either single crystalline or polycrystalline. Single-crystal nanobars and NRs originate from single crystal seeds whereas decahedral palladium seeds can grow into five-fold twinned NWs or NRs depending on their aspect ratio.[12] Another class of palladium NWs is known in the literature by different names such as wavy NWs, nanochain networks (NCNs), twisted NWs, or NW networks (NWNs). Unlike NWs or NTs, which are generally formed by templating or selective surface passivation, these materials are most often formed by self-assembly (Fig. 1).[8,13]

## Physical methods of palladium-based nanowire synthesis

### Electron/Ion beam induced deposition (EBID/ IBID) methods

The main advantage of these methods is their ability to produce 3D structures in a single step. High energy focused ion or electron beams are used to control interparticle distances and control dimensions of nanostructures. Both of the techniques are carried out in a vacuum where injected precursor is adsorbed on the surface of substrate and then a focused beam is used to produce the desired nanostructures.[3] Variations of these techniques have been used by many researchers to make single palladium NWs and test their properties. Yeonho et al.[14] used e-beam lithography to fabricate individual Pd NWs with diameters between 70-85 nm. Similarly, Bhuvana et al.[15] used e-beam writing to fabricate 30 nm diameter palladium NWs using palladium hexadecylthiolate as a negative tone direct-write electron resist. A Si substrate was coated with a 60 nm film of the above negative resist and a 5kv electron beam was used to write the desired pattern. After e-beam exposure, the substrate was developed in toluene followed by heating in ambient air. The palladium NWs fabricated using this technique had specific resistivity of 0.3 μΩm, which was close to the bulk value of 0.105 μΩm. Halfpipe palladium NTs were recently synthesized using electron beam deposition by Cho et al.[16] PVA nanofiber bundles were electrospun on a conductive substrate followed by palladium deposition using electron beam on top of the PVA nanofibers template. Half-pipe shaped Pd NTs were obtained upon dissolving the PVA nanofibers. Several similar techniques have been demonstrated to synthesize palladium NWs, but these techniques are unlikely to produce large quantities of freestanding nanomaterials at

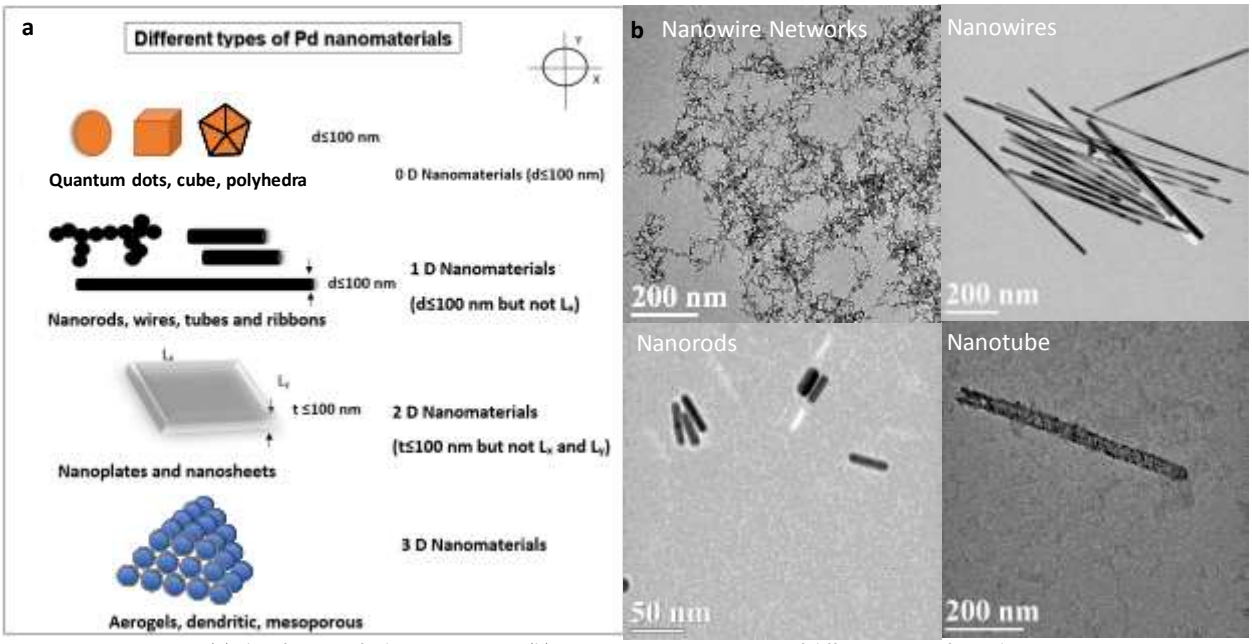


**Fig. 1** (a) Classification of Pd nanostructures. (b) Representative TEM images of different types of 1D Pd nanostructures.

reasonable cost. They are most useful for demonstrating single-NW device structures on a substrate where controlling the size and position of the NW is essential.

**Lithographically Patterned Nanowire Electrodeposition (LPNE)**

The main disadvantage of EBID and IBID fabrication strategies is that they are relatively slow and expensive, and not well suited for fabrication of an array of NWs. To overcome this limitation, a variety of nanolithographic methods have been developed, including Electrochemical Step Edge Decoration (ESED),[17] ultralarge-area block copolymer lithography,[18] crack-defined shadow mask lithography,[19] and others[20,21]. Of the above methods, LNPE has gained popularity because of the ease of fabrication and versatility it provides. LNPE is a method of fabricating polycrystalline metal NWs using electrodeposition and it combines attributes of photolithography with more versatile bottom-up electrochemical synthesis.[22] NWs produced by LNPE have a rectangular cross-section with a well-defined width and height.

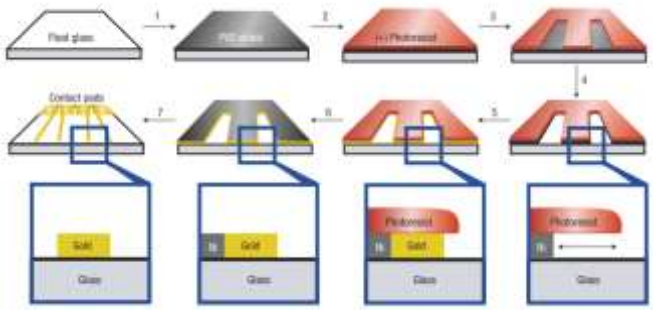

**Fig. 2** Seven-step process flow for metal-nanowire fabrication using LPNE. Reproduced with permission.[171] Copyright 2006 Springer Nature.

Xiang et al.[23] demonstrated the use of LPNE to fabricate continuous metallic (Au, Pd, Pt, Bi) NWs up to 1 cm in length. LPNE is a -7-step procedure in which a sacrificial metal (Ag or Ni) is first deposited on the surface of a silica-coated substrate

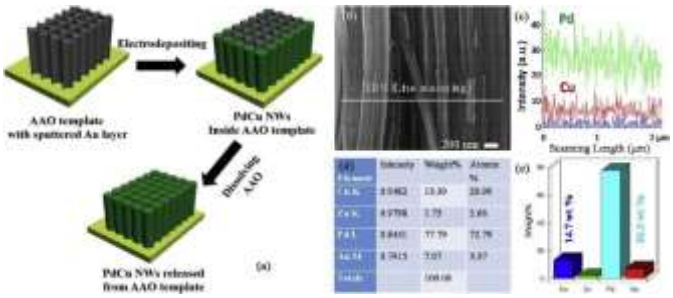


**Fig. 3.** (a) Schematic of Pd/Cu NW array fabrication, (b) SEM image of Pd/Cu NW arrays. The inset line indicates the position where the EDS line scan was taken. (c) The corresponding elemental mapping from (b). (d-e) The summarized elemental analysis of Pd/Cu NWs, obtained from the EDS line scan in (b). Zn and Au are from the substrate holder and the Au layer sputtered onto the AAO template, respectively. Reproduced with permission.[37] Copyright 2019 Springer

followed by spin coating of a photoresist layer. A UV light source is used for patterning, and the exposed nickel is etched away using nitric acid. This procedure creates a horizontal trench where a metal like Pd, Ag, Au, or Bi is electrodeposited to form NWs. Li et al.[24] studied hydrogen detection properties of platinum(Pt)- modified Pd NWs with dimensions of 40nm (h) x 100 nm (w) x 50 µm (l). The Pd NWs were fabricated using the LNPE procedure above with a thin layer of Pt electrodeposited on the surface of the Pd NW to investigate their resistance change in the presence of hydrogen. In more recent work, Koo et al.[25] demonstrated the fabrication of an array of Pd NWs with an average diameter of 200±50 nm using the LPNE procedure.

**Electrochemical deposition**

Electrodeposition is a simple and cost-effective method for preparing NWs and NRs. The process generally involves the

use of a two- or three- electrode cell setup, in which the electrolyte generally serves as the Pd source. The rate of deposition can be controlled by varying the current density or electrochemical potential of the cell. Another advantage of this method is that the nanostructures are free of capping agents and thus have bare surface available for catalytic or sensing applications. Walter et al.[26] reported an electrochemical method synthesizing NWs with diameters ranging from a few tens of nm to 1μm and lengths up to 1 mm. They used this method to prepare NWs at the step edges present on a graphite surface. Xiao et al.[27] reported the synthesis of palladium NRs by changing the concentration of palladium precursor salt ($PdCl_2$) in solution. Pd sheet was used as a counter electrode, and Ag/AgCl (0.1 M NaCl) served as a reference electrode. They observed that morphology of Pd nanoparticles was dependent on the concentration of $PdCl_2$ used and that their shape changed from Pd nanoparticles of 5-8 nm diameter to Pd NRs with uniform diameter of ~5 nm and aspect ratio of ~8, when concentration of $PdCl_2$ was increased from $10^{-5}$ M to $3x10^{-4}$ M. Most often, the electrodeposition technique is used along with either electron\ion beam methods or lithographic methods to fabricate single\array NW electronic devices. Yang et al.[28] combined electrodeposition with LNPE technology to fabricate Pd NWs with a rectangular cross-section ranging from 11-48 nm in height and 36-93 nm in width. Pd NWs of grain diameter 5 nm (nc5-Pd) and 15 nm (nc15-Pd) were electrodeposited using different deposition potentials and electrolyte compositions. In more recent work, Das et al.[29] synthesized Pd NRs using electrochemical deposition with ITO plates as working electrodes and an electrolyte solution containing 5 mM $H_2PdCl_4$ and 150 mM nicotinamide adenine dinucleotide ($NAD^+$) in 0.5 M $H_2SO_4$. $NAD^+$ served as a shape-regulating agent, and Pd NRs were deposited onto the ITO glass surface at a potential of -0.2 V for 2000 s. The synthesized NRs had an average length of 150 nm and proved to be an effective electro catalyst for methanol and hydrazine electro-oxidation.

**Hard Template-Assisted Synthesis**

Template-assisted synthesis can provide a convenient alternative to the patterning methods described above for synthesis of NWs of uniform dimensions, because the template dimensions control the shape and size of NWs and allow production of a dense array of NWs over a relatively large area.

**Mesoporous silica assisted synthesis.** Metal NWs can be prepared in good yield using silica template materials with pore sizes between 2-30 nm. Lee et al.[30] reported a size controlled synthesis approach for palladium NWs using hexagonal mesoporous silica (SBA-15) as well as mesoporous silica with varying pore sizes (CnMCM-41, n=16, 22) as templates. They used chemical vapor infiltration (CVI) to load precursor into the template matrix followed by thermal decomposition to generate Pd NWs. The Pd NWs were then separated from the template by HF etching of the silica and collected by centrifugation. The Pd NWs had diameters of 8.8, 3.7, and 4.6 nm, respectively, with lengths varying from 50 to a few hundred nm. Wang et al.[31] were able to prepare a thin film of palladium NWs using electrodeposition into a mesoporous silica template. In the same year, Fukuoka et al.[32] reported the synthesis of palladium NWs and nanoparticles using mesoporous silica (FSM-16 and HMM-1) templates. They prepared Pd NWs by photoreduction and subsequent $H_2$ reduction of impregnated $H_2PdCl_4$, while Pd nanoparticles were obtained from a single-step reduction using only $H_2$. In more recent work, SBA-15 based *in situ* synthesis of Pd NRs was reported by Li et al.,[33] who pretreated SBA-15 overnight with $Na_2PdCl_4$ and then reduced the Pd salt with ethylene glycol (EG) in an ultrasonic bath. The obtained Pd NRs were 15.96±3.89 nm in length and had an average diameter of 5.69 nm.

**Porous Anodized Aluminium Oxide (AAO) Template-Assisted Synthesis.** AAO nanotemplates allow one to conveniently synthesize large arrays of Pd NWs. The tunable pore dimensions, excellent thermal stability, and mechanical strength provided by AAO make it a desirable template for nanowire synthesis. This method requires electrical contact between the pore (NWs in later stages) and substrate, and a conductive layer is generally deposited on the substrate prior to NW growth.[34] Xu et al.[35] fabricated highly ordered Pd NW arrays using the AAO template-electrodeposition method. Porous AAO templates were prepared using aluminium foil with a two-step anodization procedure. The AAO template with a pore diameter of ~80 nm was then attached to a glassy carbon electrode, and palladium NWs were electrodeposited on the template using an aqueous solution of $Pd(NH_3)_4Cl_2$. The obtained Pd NWs were uniform with an average diameter of 80 nm and length of 800nm.

In work by Yang et al.,[36] palladium and copper superlattice NWs with different shapes (random-gapped, screw-threaded, and spiral shape) were synthesized using electrochemical deposition inside nanochannels (~70 nm in diameter) of AAO templates followed by etching. To prepare the PdCu superlattice NWs, AAO templates were prepared with their pores blocked by a thick Au layer that served as an electrode. Electrodeposition was then carried out in an electrolyte containing $Pd(NH_3)_4Cl_2$, $Na_3C_6H_5O_7.2H_2O$, $CuSO_4.5\ H_2O$ and $H_3BO_3$. The pre-contoured NWs were placed in a solution containing $CuCl_2$ with pH of 3 maintained using HCl. Finally, different shapes like random-chapped, random gapped, screw-threaded, and spiral shapes were achieved by etching at different time intervals of 20 min, 25 min, 15 min, and 25-35 min at 50°C, respectively.

Another example of Pd/Cu NW array synthesis using an AAO template was demonstrated recently in work by the same group (Fig.3).[37] Freestanding Pd NW arrays were prepared by electrodepositing Pd and Cu inside the nanochannels of an AAO template.[36] An aqueous solution of $PdCl_2$, $CuSO_4.5H_2O$ and $H_3BO_3$ was used as an electrolyte, and the electrodeposition was conducted under a constant voltage of

1.5-2.5 V onto a gold layer which was sputtered on one end of the AAO.

## Chemical methods of palladium-based nanowires

**Table 1**: Summary of Pd-based nanowires and nanotubes fabricated using lithographic and hard templating methods and their applications

| Compound | Structure | Synthesis Approach | Application | References |
|---|---|---|---|---|
| Pd | NTs | AAO Template | Formic acid and formate oxidation | 7 |
| Pd/Cu | Pd/Cu NWs | AAO Template | Hydrogen sensors | 37 |
| Pd/SBA-15 | NRs | Mesoporous silica assisted synthesis | Suzuki coupling reaction | 33 |
| PdBI | NWs | AAO template | Hydrogen sensors | 21 |
| Pd | NTs | Electrochemical deposition | Hydrogen sensors | 16 |
| PdPt | NWs | LNPE | Hydrogen sensors | 137 |
| Pd-Co | NWs | AAO template followed by chemical etching | Methanol electro-oxidation | 113 |
| Pd | NRs | Electrochemical deposition | Methanol and Hydrazine electro oxidation | 29 |
| Pd | NWs | AAO Template | Hydrogen storage | 147 |
| Pd@Zif-8 | NWs | LNPE | Hydrogen sensors | 25 |
| PdAg | Hollow Pd/Ag composite NWs | LNPE/Galvanic Replacement | Hydrogen sensors | 136 |
| Pd-Pt | NWs | LNPE/Electrodepostion | Hydrogen sensors | 24 |
| PdCu | NWs | AAO Template | Hydrogen sensors | 36 |
| Pd | NWs | AAO Template | Suzuki coupling reactions and 4-nitrophenol (4-NP) reduction | 125 |
| Pt/Pd | NTs | AAO Template | Methanol Oxidation | 77 |
| PdAu | NTs | AAO Template | Ethanol Oxidation | 172 |
| Pd | NWs | AAO Template | Suzuki coupling reaction | 125 |
| PdAu. PdPt | NWs | Polycarbonate membrane as Template | Oxygen Reduction Reaction | 119 |
| Pd | NWs | AAO Template | Formaldehyde sensor | 173 |
| Pd | NWs | Filter membrane as Template | Hydrogen sensors | 135 |
| PdNi | NWs | AAO Template/Acid etching | Anode catalyst for direct formic acid fuel cells (Electro-Oxidation of Formic Acid) | 109 |
| Pd | NTs | AAO Templates with CdS | Glucose sensors | 146 |
| Pd | NWs | LPNE | Hydrogen sensors | 132 |
| Pd | NWs | LNPE | Hydrogen sensors | 130 |
| Pd | NRs | Electrochemical deposition | Ethanol Oxidation | 174 |
| Pd | NWs | DEA | Hydrogen sensor | 20 |
| Pd | NRs | Electrochemical deposition | Oxygen Reduction Reaction | 27 |

In more recent work, Ding et al.,[7] fabricated mesoporous Pd NT (P-PdNTA) arrays using a dual-template procedure. AAO served as a hard template whereas phyantriol served as a soft template. To synthesize P-PdNTA, one end of AAO was sputtered with gold to form a conductive layer as well as to serve as a seed for Pd nucleation. Then a vacuum filling process was used to uniformly coat phytantriol on the inner nanochannels of AAO, which was then placed on an ITO glass substrate that served as a working electrode. The electrodeposition used platinum wire as counter electrode and saturated calomel electrode (SCE) as a reference electrode. $PdCl_2$ was used as the electrolyte. The electrodeposition was carried out for 30 minutes with 0.3V SCE potential bias. The synthesized P-PdNTA had a uniform diameter of ~400 nm and a wall thickness of ~12 nm. Table 1 summarizes work done on Pd NWs fabrication using the above-mentioned method along with their application.

## synthesis

Although palladium NWs can be synthesized using the top down techniques discussed above, most of these techniques are still very costly and require further development to reproducibly synthesize the large quantities of NWs for applications such as electrocatalysis and hydrogen storage that require bulk quantities of NWs, as compared to sensing applications, which may have much lower material requirements. Bottom-up solution-phase synthesis methods can produce palladium NWs in good yield and in much larger quantities. Palladium is not inherently anisotropic and hence requires capping agents or some kind of template to grow in one dimension. Palladium is a noble metal with a face-centered cubic (fcc) lattice structure that can be prepared in the form of nanostructures of various shapes. Solution phase synthesis of palladium nanoparticles starts with nucleation, which is defined as the formation of small clusters or seeds

with a well-defined crystallinity and stable structure. Once the seeds nucleate, if they are single crystal seeds, they can grow into several possible shapes like cubes, octahedra, and cuboctahedra, based on passivation of particular crystalline facets.[38] Single crystal seeds often form multiple twinned structures to reduce total surface energy. Five-fold twinned particles may adopt an icosahedral or decahedral geometry, and may then go on to grow into five-fold twinned palladium NRs and NWs. [12,39]

Using different reaction conditions, researchers have been able to synthesize palladium nanomaterials bounded by with different facets. 1D nanomaterials are often formed by a combination of different facets.[40] Some of the strategies for achieving 1D growth of palladium in solution include polyol synthesis, galvanic replacement, chemical reduction, templated synthesis, and seed-mediated synthesis.

**Polyol synthesis**

The polyol method is one of the most widely used solution phase synthesis routes for achieving 1D growth of metallic nanocrystals. The polyol synthesis produces metallic nanoparticles in high-boiling, multivalent alcohols. Polyols are organic compounds with multiple hydroxyl groups such as ethylene glycol (EG), diethylene glycol (DEG), triethylene glycol (TEG),1,2-propylene glycol and 1,5-pentanediol. Polyol synthesis uses one of the polyols as both solvent and reducing agent. One of the main advantages of polyols is their water-like ability to dissolve low-cost, water-soluble salts like halides, nitrates, and sulfates, combined with much higher boiling point temperatures than water.[41]

For palladium NW synthesis using polyol methods, a palladium salt solution is injected into a refluxed polyol solution containing a capping agent to prevent agglomeration and provide surface passivation to enable 1D growth of NWs. EG and DEG are the most widely used polyols, while capping agents like polyvinyl pyrrolidone (PVP) and cetyltrimethylammonium bromide (CTAB) along with halide salts (NaCl, NaI, KBr, etc.) that act as co-surfactants are used to promote 1D growth.

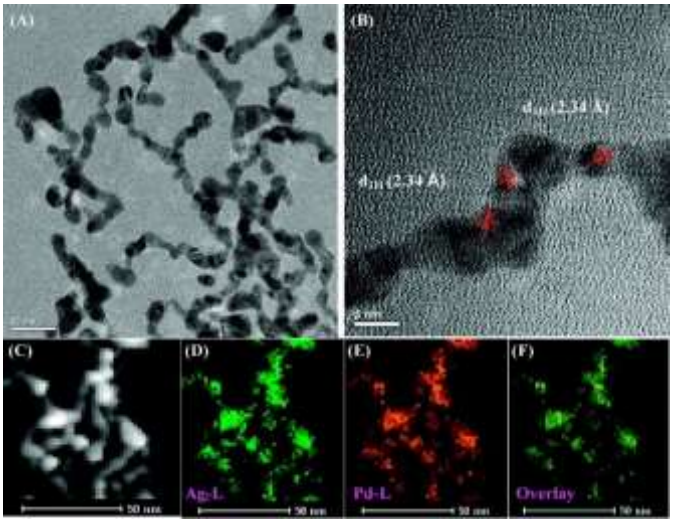


**Fig. 4.** A-B) High-resolution TEM micrographs of PdAg nanowires at different magnifications. The scale bars are (A) 20 nm and (B) 5 nm. (C) High angle annular dark field (HAADF) STEM image of PdAg nanowires and the corresponding elemental mapping of Ag (D), and Pd (E). (F) Overlay map of the elements in the PdAg nanowires. Reproduced with permission.[42] Copyright 2012 American Chemical Society

To date, several types of palladium and palladium alloy NWs have been prepared using polyol synthesis. Lu et al.[42] reported a facile one-pot polyol synthesis of PdAg alloy NW networks in which EG was used as solvent and reducing agent and PVP was the capping agent. In their work, 0.6 mmol of PVP was dissolved in 5 ml of EG and heated to 170°C, then an equimolar (0.05 mmol) mixture of $Pd(NO_3)_2$. 2 $H_2O$ and $AgNO_3$ dissolved in water was rapidly injected into the heated EG solution (Fig.6 a). The reaction was stopped after 1 hour, the solution was cooled to room temperature, and the particles were collected, washed, and re-dispersed in water. These NWs had an average diameter of 5-8 nm and were up to 200 nm in length (Fig.4). In similar work, intermetallic $Pd_3Pb$ NW networks were synthesized by Shi et al.[43] For NW synthesis, $Na_2PdCl_4$, $Pb(acac)_2$, PVP, and citric acid were dissolved in EG, then heated to 170°C for one hour to produce an interconnected network of NWs with an average diameter of 7.8±1.8 nm.

Huang et al. [44] reported the synthesis of straight, penta-twinned palladium NWs by a one-pot polyol synthesis method using DEG as solvent and reducing agent. Ascorbic acid was used as a co-reducing agent, and NaI served as co-surfactant along with PVP. These reagents were heated to 160°C, then $Na_2PdCl_4$ in DEG was quickly injected. The reaction continued for an hour before it was rapidly quenched using an ice-bath. The obtained NWs had an average length of 720 nm and an average diameter of ~8 nm (Fig.5 A, B). The HAADF-STEM images (Fig 5 C, D) reveal the uniform diameter and presence of a penta-twinned structure respectively. High-Resolution TEM imaging (Fig.5 E) shows lattice fringes with spacings of 0.23 and 0.2 nm, corresponding to {111} and {200} planes of fcc Pd. Existence of twinned structures was further confirmed by the fast fourier transform (FFT) pattern (Fig.5 F) showing two sets of diffraction patterns corresponding to <110> and <111> zones of Pd nanocrystals.

**Hydrothermal/Solvothermal Synthesis**

Hydrothermal/solvothermal synthesis refers to chemical reactions carried out in a sealed, heated reactor above ambient temperature and pressure (Fig 6 b). [45] When the solvent is water, this approach is called hydrothermal synthesis; for other solvents, it is called solvothermal synthesis. Several Pd-based nanostructures including Pd and Pd-alloy NWs have been synthesized in good yield using hydrothermal or solvothermal synthesis.

Huang et al.[46] reported hydrothermal synthesis of five-fold twinned Pd NWs and NRs with high aspect ratio in a Teflon-lined stainless-steel autoclave at 200 °C for 2 hours with PVP as both reducing agent and capping agent. NaI served as a co-surfactant in this case. The Pd NWs had a uniform diameter of 9±1 nm and were up to 3 μm in length. Without NaI, the reaction yielded networked Pd NWs. Doubling the concentration of PVP resulted in spherical particles. When the reaction time was extended to 24 hours, Pd NWs ripened into more thermodynamically stable spherical particles. Lu et al.[47] reported the synthesis of 5-fold twinned Pd NWs using the hydrothermal route. Instead of using a trace amount of Cu or

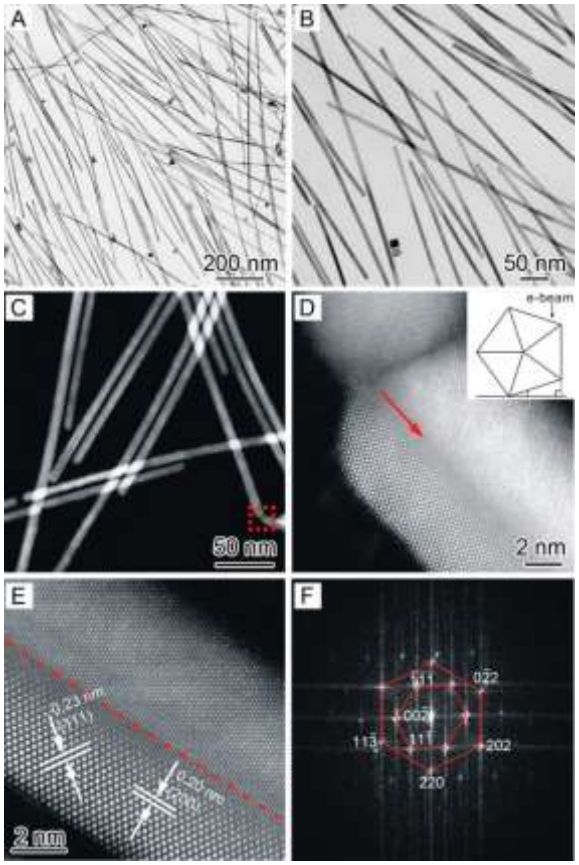


**Fig. 5.** Morphological and structural characterization of Pd NWs at different magnification. (A, B) TEM images at low and high magnifications, respectively, and (C) HAADF-STEM image. (D, E) HRTEM images of the region marked by a dashed box in panel C and the middle section of a nanowire, respectively. The red arrow and dotted line indicate the twin boundary running along the long axis of the nanowire. The inset in panel D illustrates the orientation of the electron beam relative to the nanowire. (F) Fourier transform pattern derived from the lattice fringes in panel E. Reproduced with permission.[44] Copyright 2017 American Chemical Society

Ag salt solution, they utilized small organic molecules to tune the extent of oxidative etching. They harnessed the interaction between small organic molecules like acetonitrile ($CH_3CN$) and $Cl^-$ ions to promote the growth of penta-twinned seeds, which later grew into NWs. To synthesize Pd NWs, NAI, PVP(K30), ultrapure water, and $CH_3CN$ were sonicated in a vial, then $NaPdCl_4$ solution was added, followed by HCHO solution. The mixture was transferred into a Teflon-lined reactor and heated to 140 °C for 4 to 12 hours to produce Pd NWs with an average diameter of 15.4 nm and an average length of 490 nm. Upon replacing acetonitrile with an equal volume of acetone, 1-4-dioxane, or half the volume of 1,3,5-trioxane, similar results were obtained.

Yang et al.[48] reported hydrothermal synthesis of palladium-iridium NWs using PVP. They dissolved $PdCl_2$, $(NH_4)_2IrCl_6$, NaI, and PVP in 12 ml DI water and stirred at 50 °C for 3 hours to form a homogeneous mixture. They transferred the solution to a 25 ml Teflon-lined stainless-steel autoclave reactor and heated it to 210 °C for 2 hours. In their later work, Yang et al.,[49] found that the morphology of nanoparticles changed from NWs to nanodendrites depending on the concentration of Pd and Ir precursor salts. They observed that upon increasing the concentration of iridium, the morphology of their nanoparticles changed from NWs ($Pd_2Ir_1$) to

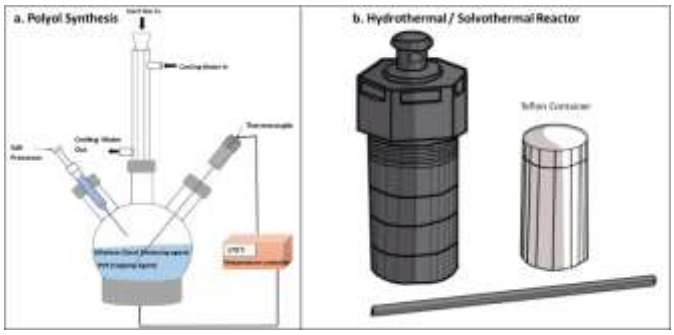


**Fig. 6** Schematic representation of (a) polyol synthesis using a 3-neck flask. (b) hydrothermal/ solvothermal reactor.

nanodendrites ($Pd_1Ir_2$). More recently, Yan et al.[50] reported synthesis of PdCu alloy NWs using a one-pot solvothermal synthesis route with EG and dimethylformamide (DMF). $H_2PdCl_4$ solution was mixed with varying amounts of $CuCl_2.H_2O$

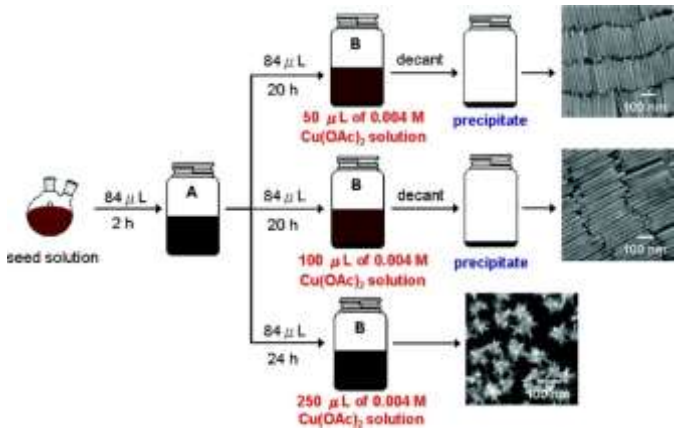


**Fig. 7** Experimental procedure used to make palladium nanorods and branched nanocrystals. Reproduced with permission.[53] Copyright 2009 American Chemical Society

in water and added to a 15 ml vessel containing PVP dissolved in a DMF/EG mixture. After sonication of the mixture, it was heated in an autoclave reactor at 170 °C for 8 hours. When the same reaction was carried out in the absence of Cu, granules with an average particle size of 11 nm were obtained. In the presence of Cu, the tiny granules were interconnected in a wire-like morphology as confirmed by TEM images. These results suggest that an appropriate amount of Cu assists in the formation of self-supported Pd-Cu NWs.

**Seed Mediated synthesis**

Seed-mediated synthesis has been widely used to synthesize Au and Ag NRs.[51] One of the main advantages of this method is its ability to fine-tune the dimensions of NRs. It starts with the synthesis of metal nanocrystal seeds, typically 3-4 nm in diameter, using a strong reducing agent (generally $NaBH_4$) in the presence of a capping agent. The next step involves 1D growth of the seeds in a solution containing metal salt, a weak reducing agent (e.g., ascorbic acid) and a capping agent and structure directing agent (e.g., cetyltrimethylammonium bromide, CTAB). The metal seeds serve as a nucleation site, while CTAB or another structure-directing agent guides the

growth into 1D nanomaterials whose diameter largely depends on the dimensions of the seed. Berhault et al.[52] demonstrated the synthesis of palladium nanoparticles of different morphologies using a seed-mediated approach. They discovered that palladium NRs synthesized using a seed-mediated approach had 5-fold symmetry, similar to Ag and Au NRs prepared by the same strategy. The synthesis involved two steps, starting with palladium seed production using aqueous $Na_2PdCl_4$ and CTAB. Rapid addition of an ice-cold aqueous solution of $NaBH_4$ initiated nucleation of seeds. The Pd seeds were then used with $Na_2PdCl_4$, sodium ascorbate, and varying amounts of CTAB to obtain different Pd nanoparticle morphologies.

Chen et al.[53] used a seed-mediated approach to synthesize palladium NRs and branched nanocrystals. Uniform palladium NRs with average lengths of ~200 and 300 nm and average diameter of ~20nm were obtained using a trace amount of copper acetate. Upon increasing the amount of copper acetate, branched Pd nanocrystals were obtained (Fig.7). Addition of other metal salts like $Zn(OAc)_2$, $Ni(OAc)_2$ and $AgNO_3$ produced faceted nanoparticles rather than rods. $Cu(NO_3)_2$, $CuCl_2$, and $CuSO_4$ produced similar results to copper acetate, indicating that the presence of Cu ion and not acetate was crucial for formation of Pd NRs.

Huang et al.[54] used Pd NRs prepared by seed-mediated synthesis as a template for producing bimetallic or hollow nanostructures. Pd decahedral seeds of ~6.5 nm diameter were prepared using PVP, and $Na_2SO_4$ as surfactants with DEG as both solvent and reducing agent. To prepare Pd NRs, PVP, AA, and NAI were added to a vial containing DEG and heated to 160 °C. Pd seeds were added, followed by $Na_2PdCl_4$. The reaction was cooled in an ice bath after 1 hour. Using the resulting Pd NRs as a template, they then produced Pd-Pt bimetallic NTs and Pd@Au core-shell NRs.

Apart from palladium NRs, NWs have also been synthesized using the seed-mediated approach.[55] Au seeds were used to prepare palladium NWs stabilized by thiol-functionalized ionic liquid (TFIL). 1-methylimidazole, 1-chloro-2-ethanol, and mercaptoacetic acid were used as starting materials for the TFIL. TFIL-stabilized Au seeds of ~2.2 nm diameter were synthesized using $NaBH_4$ as reducing agent. The seeds were mixed with $H_2PdCl_4$ under vigorous stirring, followed by addition of excess $NaBH_4$ at room temperature. HRTEM and TEM images showed polycrystalline NWs comprised of fcc nanocrystals. Core-shell structures formed upon increasing or decreasing the concentration of nanogold seeds, indicating the importance of seed concentration.

**Soft Template-Directed Synthesis**

One-dimensional growth of nanostructures can also be achieved *via* a template-directed approach in which a soft template serves as a scaffold for the growth of NWs around it or within it. In contrast to hard templates like AAO discussed in section 3.1.4 above, soft templates are micelles assembled from surfactants or biotemplates such as DNA or microorganisms. Unlike hard templates in which the template structures are pre formed, soft templates are generally assembled in the reaction medium, driven by interactions of surfactants with the solvent and one another. When the concentration of surfactant molecules exceeds a critical value, they spontaneously arrange themselves into micelles or inverse micelles (Fig 8).[56] For appropriate combinations of surfactant and solvent identity and concentrations, cylindrical

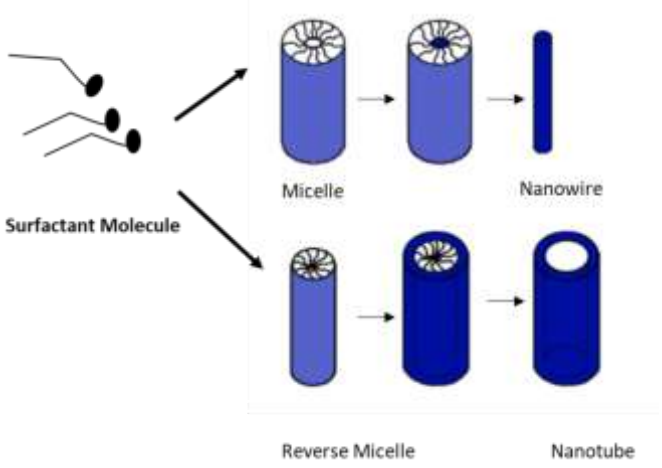


**Fig.8** Schematic illustrations showing the formation of nanowires and nanotubes by templating against mesostructures self-assembled from surfactant molecules. Adapted with permission.[56] Copyright 2003 Wiley-VCH

or rod-shaped micelles form, which can guide the growth of NRs or NWs.

**Surfactant-based soft templates.** Ksar et al.[57] demonstrated the synthesis of palladium NWs using a quaternary system comprised of aqueous $Pd(NH_3)_4Cl_2$, CTAB (surfactant), pentanol (co-surfactant) and cyclohexane (oil phase). Electron beam irradiation induced fast radiolytic reduction and formation of NWs with diameters of ~20 nm and lengths of a few tens of nm. Upon increasing the concentration of co-surfactant, the length of NWs slightly increased. When the experiment was performed without co-surfactant, spherical Pd particles of 5-6 nm were obtained. In the same year, Jiang et al.[58] reported the synthesis of polycrystalline Pd NWs using PVP as a soft template. In their synthesis, Pd nanoparticles were generated first using Cu as a reducing agent. These nanoparticles assembled into 1D structures, guided by the PVP template. To obtain Pd NWs, $Pd(OAc)_2$ and PVP were dissolved in methanol followed by addition of copper powder and heating for 24 hours at 50 °C. This method produced polycrystalline NWs with an average diameter of 100 nm. The amount of PVP used was crucial to getting 1D NWs; Pd particles of 5 nm average diameter were obtained when the amount of PVP was reduced.

In contrast to the work by Jiang et al.,[58] in which the Pd NWs were polycrystalline, Siril et al.[59] demonstrated the synthesis of monocrystalline Pd NWs of high aspect ratio using hydrazine vapor to reduce $Pd_2(DBA)_3$ within a hexagonal mesophase stabilized by CTAB. The Pd NWs were collected by centrifugation after addition of 2-propanol to destabilize the mesophase. Imura et al.[60] synthesized Pd NW networks and bimetallic Pd-Ni NWs using a soft template formed by long-chain amidoamine (C18AA) and slow reduction. They mixed a toluene solution of CTAB with aqueous $K_2PdCl_4$ to achieve phase transfer of Pd from water to toluene. The Pd-containing toluene was mixed with C18AA in toluene and stirred for 2 hours, followed by addition of $NaBH_4$ solutions of varying concentration. To synthesize bimetallic NWs, the Pd solution was partly replaced with a solution of $Ni(acac)_2$, which was added along with the C18AA toluene solution. The NWs thus obtained had an average diameter of 3.5±0.4 nm.

Zhang et al.[61] reported synthesis of 3D Pd-P NW networks by a one-step soft-template-assisted method in which polyethylene glycol hexadecyl ether (Brij 58) was used to create the soft template, and $NaH_2PO_2$ was used for P doping. Gao et al.[62] reported a soft-template assisted attachment growth approach to synthesize monometallic (Pd, Pt) and bimetallic nanochain networks of compositions including Pt-Au, Pd-Au, and Pt-Pd. Dioctadecyldimethylammonium chloride (DODAC) was used by Xu et al.[63] to synthesize single crystalline Pd NWs with ascorbic acid as reducing agent. This approach was recently extended to synthesize PdPt bimetallic NWs by Lv et al.[64] DODAC can form a hexagonal mesophase through a cooperative self-assembly process due to electrostatic interactions between ammonium groups in DODAC and anionic metal precursors ($PtCl_6^{2-}$ and $PdCl_4^{2-}$). Bimetallic NWs were obtained by co-reduction of the metal precursors using AA.

Lyotropic liquid crystals are highly concentrated worm-like cylindrical micelles formed by surfactants. Their diameter can be changed by tuning the oil to water ratio, the concentration of co-surfactant, and the ionic strength of salts in an aqueous medium. Kijima et al.[65] reported synthesis of noble metal (Pt, Pd, Ag) NTs of outer diameter 6-7 nm by reducing metal salts confined within a liquid crystal formed using a 1:1 mixture of surfactants. Pd NTs were obtained by hydrazine treatment of cylindrical mesophases formed from a 1:1:1:60 mixture of $Pd(NO_3)_2$, nonaethylene glycol monodecyl ether ($C_{12}EO_9$), polyoxyethylene (20) sorbitan monostearate (Tween 60), and water. The obtained NTs had inner and outer diameters of 3 and 6 nm, respectively. Chawla et al.[66] also reported the synthesis of palladium NWs using liquid crystal templates. Bis-dibenzene acetone palladium ($Pd(DBA)_2$) in toluene was mixed with CTAB dissolved in brine. Later 1- pentanol and then SDS were added to make mesophases with CTAB. After incubating the mixture for about a week, it was reduced using $H_2$ to form palladium NWs.

**Bio-based soft templates.** Apart from surfactant-based soft templates, bio-based soft-templates have also been explored to synthesize metallic NWs. Deoxyribonucleic acid (DNA) is one of the most widely explored bio-templates for NW synthesis, mainly because it has a diameter of ~2 nm and can be up to microns in length. Ritcher et al.[67] demonstrated electroless deposition synthesis of palladium NWs using a two-step procedure. First, $Pd(CH_3COO)_2$ was sonicated in DI water, then mixed with an equal amount of DNA solution for 2 hours. The Pd NWs were deposited on the DNA surface in a second step using a reduction bath containing sodium citrate, lactic acid, and dimethylamine borane (DMAB), with ammonia to adjust the pH. This step reduces the metal ions into metal clusters attached to the DNA surface. One major drawback of this approach is that the reduction step using DMAB has very fast kinetics, which makes attaining homogeneous growth difficult, resulting in uncontrolled localized growth at some points. Nguyen et al.[68] overcame the issue of fast reaction kinetics by first achieving slow and selective PdO deposition and later reducing PdO to Pd NWs. They synthesized thin and highly conductive Pd NWs using a two-step approach. Starting with DNA attached on a substrate coated with hexamethyldisilazane (HMDS) they applied $PdCl_2$ solution, which resulted in selective precipitation of PdO on the DNA strands. Later, the substrate was immersed into a solution of an appropriate reducing agent to convert PdO into Pd NWs. Kundu et al.[69] demonstrated a photochemical method to synthesize electrically-conductive Pd NWs with an average diameter of 55-77 nm and lengths up to 3-5 µm. Their results indicated that DNA can be used as both a non-specific capping agent as well as a reducing agent for Pd NW synthesis.

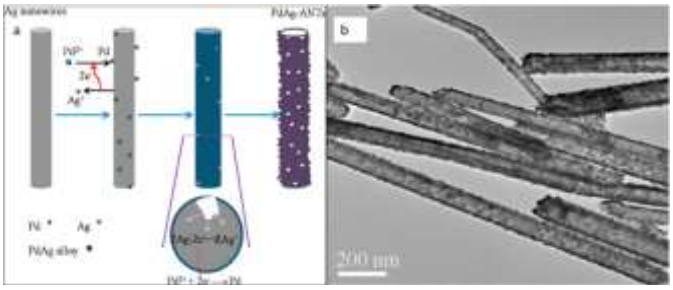


**Fig. 9** (a) Schematic illustration showing the synthesis process of PdAg alloy nanotubes via galvanic replacement of Ag nanowires. (b)TEM image of PdAg alloy nanotubes. Reproduced with permission.[69] Copyright 2017 Elsevier.

Chen at al.[70] reported the synthesis of ternary (Au/Ag/Pd) NWs using a microorganism-assisted synthesis route. To prepare NWs, dried Pichia pastoris cells (PPCs) served as biotemplates along with CTAB as a co-surfactant in DI water. The required amounts of Pd and Au salts were added first, followed by a small amount of AA as a reducing agent along with the injection of Ag salt solution using a syringe pump. The solution was kept at 60 °C for 3 hours, and the composite NWs were collected by centrifugation and dried in a vacuum oven.

**Galvanic Replacement**

NW synthesis *via* galvanic exchange reactions can produce NWs of materials that are not inherently anisotropic. One of the advantages of this method is that the shape and size of NWs can be tuned based on those of the sacrificial NW template used. One of the most widely used sacrificial NW templates is Tellurium (Te).[71] Liang et al.[71] used ultrathin Te

NWs of very high aspect ratio to form Pd NWs *via* galvanic exchange, using EG as solvent at 50°C. Zhu et al.[72] reported the synthesis of PdM (M=Pt, Au) bimetallic alloy NWs using Te NWs as sacrificial templates. They also studied the effect of solvent on the final product and found that when EG was replaced with water, the reaction kinetics were faster. PdPt and PdAu NWs were obtained when the galvanic reaction was carried out at room temperature in aqueous solution. Hong et al.[73] reported the synthesis of PdTe NWs by a Te template-based route and used ascorbic acid as a reducing agent to get a high yield of PdTe NWs. In more recent work, Sahoo et al.[74] prepared entangled Pd NWs *via* galvanic replacement of long Te NWs. The resulting high aspect ratio Pd NWs were retained on a membrane surface as a thin porous film, and used as a continuous-flow catalytic reactor. Apart from Te NWs, other metal NWs have also been used as templates for 1D Pd nanostructures. Palladium NTs have been synthesized by galvanic displacement from sacrificial templates of Ag NWs (Fig. 9),[75 76] and ZnO NWs.[77 78]

**Chemical reduction methods**

Synthesis of NWs by chemical reduction methods is gaining popularity because of its simplicity and low preparation cost. Unlike polyol and hydrothermal synthesis, which require high temperature, chemical reduction methods are most often carried out at room temperature in aqueous media, which not only reduces the cost of production but also reduces solvent waste. In such synthesis, a very strong reducing agent like $NaBH_4$ or hydrazine is added into an aqueous Pd salt solution with an appropriate quantity of capping agent to form 1D palladium nanostructures. A small amount of halide is often added as a co-surfactant, and is found to promote formation of 1D structures.

Lan et al.[79] reported the synthesis of Pd nanochain networks with ultra-low loading of Pt using a facile aqueous synthesis route with hydrazine as a reducing agent. Pd nanochains were first synthesized using an aqueous solution of $PdCl_2$ and PVP at pH 7, followed by addition of hydrazine. To load the Pd nanochains with a small amount of Pt, the Pd nanochains were dispersed in an aqueous solution of $H_2PtCl_4$, which displaced surface Pd atoms of nanochains. Yuan et al.[80] reported the synthesis of self-supported AuPd alloy NW networks using a naturally occurring organic chemical, theophylline, as capping and structure directing agent with hydrazine as a reducing agent.

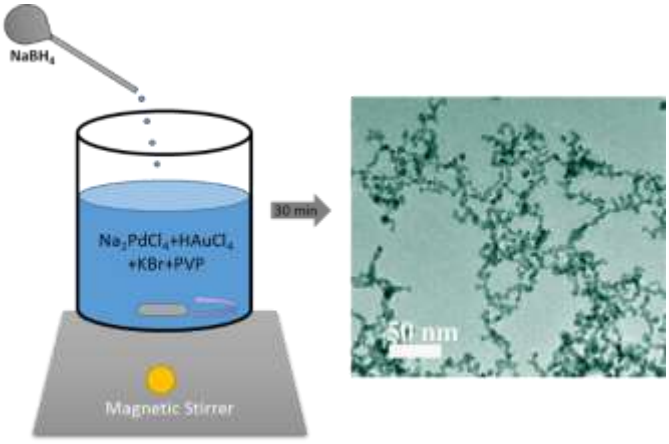


**Fig.10** Schematic of PdAu nanowire networks synthesis using chemical reduction method; (b) TEM images of PdAu nanowire network. Adapted with permission.[82] Copyright 2014 American Chemical Society

Template-free formation of Pd NW networks was reported by Wang et al.[81] The Pd NWs were synthesized by a self-assembly process using trisodium citrate as a capping agent and $KBH_4$ as reducing agent. Hong et al.[82] reported a facile synthesis of bimetallic PdAu NW networks using a chemical reduction method in aqueous solution. To synthesize PdAu NWs, PVP was dissolved in water, then mixed with aqueous $Na_2PdCl_4$ and KBr. $NaBH_4$ was added as a reducing agent to produce networks of NWs with an average diameter of 5 nm (Fig.10).

Apart from $NaBH_4$ and hydrazine, a few other reducing agents have been used to synthesize Pd-based NW networks. Li et al.[83] reported the synthesis of Pd NW network using ethylenediaminetetraacetic acid (EDTA) as a reducing agent. EDTA limits the reactivity of Pd by forming Pd-EDTA complexes, which is crucial for NW network formation.[8] PVP acted as a structure-directing agent in this reaction and the NWs formed were 6-9 nm in diameter and tens to hundreds of nm in average length. Table 2 summarizes work done on Pd NWs following chemical based methods.

## Growth mechanism and factors affecting growth

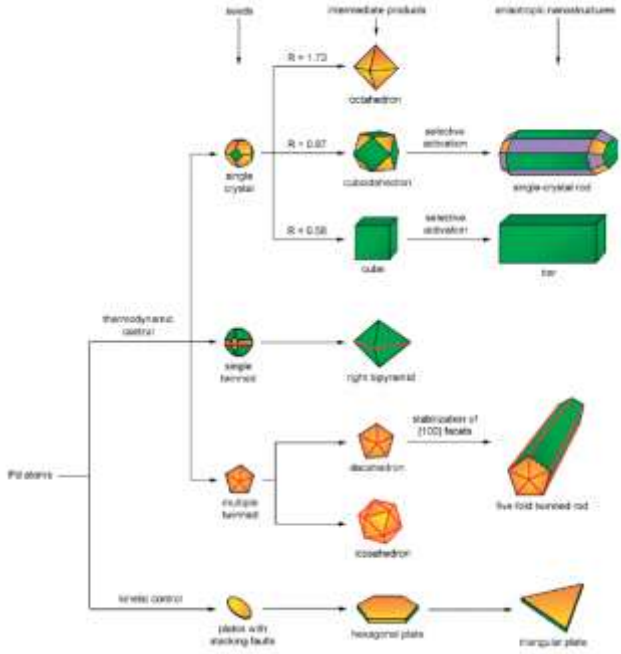

**Fig. 11** A schematic illustration different morphologies of Pd nanostructures and conditions leading to them. Reproduced with permission.[12] Copyright from Wiley-VCH.

## of nanowires

Shape controlled synthesis of palladium NWs produced *via* solution phase synthesis is a challenging task. Even though many other methods have been used to synthesize NWs, solution phase synthesis of palladium NWs is more popular

because it involves a single step and is relatively low-cost and scalable. The key challenge that researchers face is to achieve a good yield of high aspect ratio NWs. Even a slight change in the environment often results in a different product or a mixture of NWs and polyhedra.

Moreover, fast reaction kinetics make elucidating the formation mechanism of palladium NWs difficult. While some basic understanding of the formation mechanisms of 1D Pd-based materials is available, most mechanisms that have been proposed so far are either incomplete or ambiguous and require further investigation. Understanding mechanisms of formation should help in scaling up and mass production of metallic NWs for commercial application. A summary of studies done to understand the reaction mechanism of NWs synthesized in solution is presented in this section, followed by the characterization tools used to study them.

**Penta-twinned palladium NWs/NRs**

Seedless synthesis of Pd NWs in solution phase often involves three major steps, nucleation, seed generation, and growth of seeds into nanocrystals with a distinctive shape. This growth step can be affected by a variety of conditions that can be broadly classified as thermodynamic (e.g. surface capping and reduction potential) and kinetic (concentration, temperature, mass transport, and involvement of foreign species) parameters.[84] These conditions are often interrelated, and a slight change in one of the parameters can change the seeds or nuclei, resulting in products of undesired shape. Different shapes of Pd nanocrystals can be seen in Fig 11. Kinetic control can be used to synthesize 1D Pd nanostructures by slowing down the reduction kinetics of metals.

Solution phase synthesis of palladium NWs starts with nucleation, producing clusters that grow into seeds with well-defined crystallographic facets, driven by surface energy minimization. The surface energy of fcc crystal facets generally increases in the order $\alpha_{\{111\}} < \alpha_{\{100\}} < \alpha_{\{110\}}$.[85] When the seeds grow in solution, they tend to be bounded by facets with minimum energy to reduce the overall surface energy. Under thermodynamically-controlled conditions, isotropic Pd crystals bounded by {111} or {100} planes are formed, whereas anisotropic structures can be formed under kinetically-controlled conditions. Xiong et al.[38] demonstrated the synthesis of single crystal palladium NRs and nanobars. They were able to break symmetry and grow anisotropic nanostructures through a combination of three processes: 1. Speedy reduction of precursors to produce a rapid burst of atoms that generate a high concentration of Pd seeds *via* an increase in the concentration of reducing agent; 2. Preferential growth by taking advantage of localized oxidative etching of one specific crystal facet; and 3. Use of bromide as a surface passivating agent to promote the formation of {100} and {110} facets over {111} facets.

Lim et al.[86] reported the synthesis of ultra-high aspect ratio Pd NWs using PVP as a mild reducing agent and capping agent along with NaI and a trace amount of Cu salts. They observed that addition of a small amount of sodium chloride (NaCl) reduced sample preparation time by improving the solubility of $PdCl_2$ and lowered the reaction rate by forming a $PdCl_4^{2-}$ complex, which promoted diffusional 1D growth. NaI and PVP are known to promote 1D growth *via* surface passivation.[46] The addition of $Cu^{2+}$ and $Cl^-$ ions appeared to supplement the growth and prevent oxidative etching. Fig. 12 G shows schematics of the mechanism of penta-twinned Pd NW growth. They used a number of characterization tools to support their claim. First, X-ray Diffraction (XRD) studies revealed the highly-crystalline nature of Pd NWs with intensities consistent with high aspect ratio NWs. The intensity ratio between the (111) and (200) peaks was 83% higher than the standard (JCPD card) and that between the (200) and (220) peaks was 80% higher. This suggests that Pd NWs are bounded mostly by {111} and {100} facets which is typical of NWs with pentagonal geometry (Fig 12 F). Bright-field TEM further confirmed the pentagonal geometry of obtained NWs. A high-resolution TEM image of one isolated Pd NW revealed lattice fringes with a distinctive Moiré pattern. The Fast Fourier transforms (FFT) of these images were similar to other reported pentagonal twinned NRs and NWs of Ag. [87] Furthermore, the SAED image of a Pd NW cluster revealed two additional peaks at 2.72 and 3.67 Å d-spacing, which were attributed to $PdI_2$ and PVP respectively. A negative zeta potential was obtained for the samples confirming presence of iodide on the NWs, as PVP is a neutral polymer.

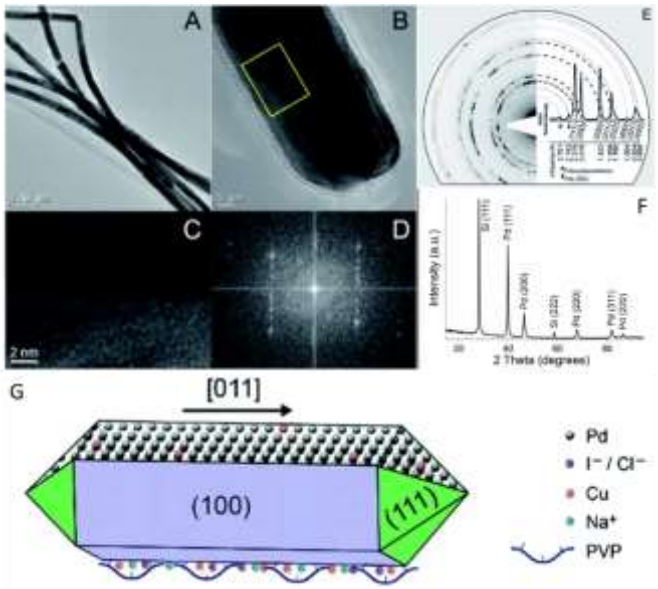


**Fig. 12** (A) Bright Field TEM image of Pd nanowire aggregate; (B) single Pd nanowire; (C) Rotated-enlarged image of rectangular area outlined in B; (D) FFT of (C); (E) Background subtracted SAED pattern (left) and with integrated intensities (right) for Pd nanowire cluster; (F) XRD pattern of Pd nanowires ; (G) Schematic of ideal Pd NW with penta-twinned cross-section, [011] growth direction, and surface coating. Reproduced with permission.[86] Copyright 2018 The Royal Society of Chemistry.

**Ultrathin Pd-based NWs in hexagonal mesophases**

Penta-twinned Pd NWs synthesized *via* polyol or hydrothermal methods often exhibit low yield and large diameter because of various reaction parameters discussed later in the paper. However, ultrathin single crystalline Pd NWs have been synthesized in high purity using a one-pot surfactant-directed route.[11,63,64] Hence, understanding the underlying mechanism of this synthesis route would be useful for scaling and extending it. Lv et al. [88] reported the synthesis of ultrathin ternary PdCuP alloy NWs using DODAC as soft-template and $NaH_2PO_2$ as a reducing agent as well as a source of P. $H_2PdCl_4$ and $Cu(NO_3)_2$ were dissolved in aqueous DODAC solution, followed by addition of $NaH_2PO_2$. The reaction mixture was heated at 95 °C for 2 hours to yield a dark brown product. The obtained NWs were ~2.5 nm in average diameter and hundreds of nanometers in length (Fig. 13 e). HAADF-STEM images showed a d-spacing of 0.219 nm, indexed to (111) plane of fcc Pd alloy nanocrystals. Slight lattice distortion was also observed, which was attributed to amorphous P dispersed within the PdCuP ternary NWs. The synthesis mechanism for this route is largely dependent on self-assembly of DODAC into

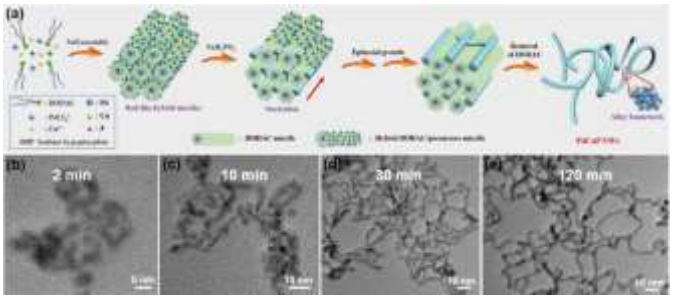


**Fig. 13** Formation mechanism of ultrathin PdCuP nanowires. (a) Schematic illustration of growth mechanism of ternary PdCuP NWs using DODAC as the surfactant template and $NaH_2PO_2$ as reducing agent and P source. Representative PdCuP alloy TEM images obtained at reaction times of (b) 2 min, (c) 10 min, (d) 30 min, and (e) 120 min. Reproduced with permission.[88] Copyright 2019 Elsevier

hexagonal mesophases which serve as microreactors for NW growth (Fig. 13 a).

**NW/nanochain network growth mechanism**

Wang et al.[81] reported the synthesis of palladium NWs *via* a self-assembly process that is governed by electrostatic forces between the particles. NW synthesis begins with nucleation, and an appropriate Pd/capping agent ratio is required to obtain a NW morphology by linear assembly of nanocrystals. If, at the initial stages, the concentration of capping agents around the nanoparticles is too high, it will inhibit self-assembly of nanoparticles into NWs. On the other hand, if the concentration of the capping agent around the nanoparticles is too low, uncontrolled aggregation of nanoparticles can occur.
A similar mechanism was reported recently by Zhang et al.[89] Palladium nanochain networks and nanodendrites were synthesized using poly-L-lysine (PLL). Fig. 14 A and B present TEM and HRTEM images of Pd NWs synthesized using PLL. The observed lattice fringe spacing of 0.234 nm corresponds to (111) crystal planes of Pd (Fig. 14 B). Upon increasing the

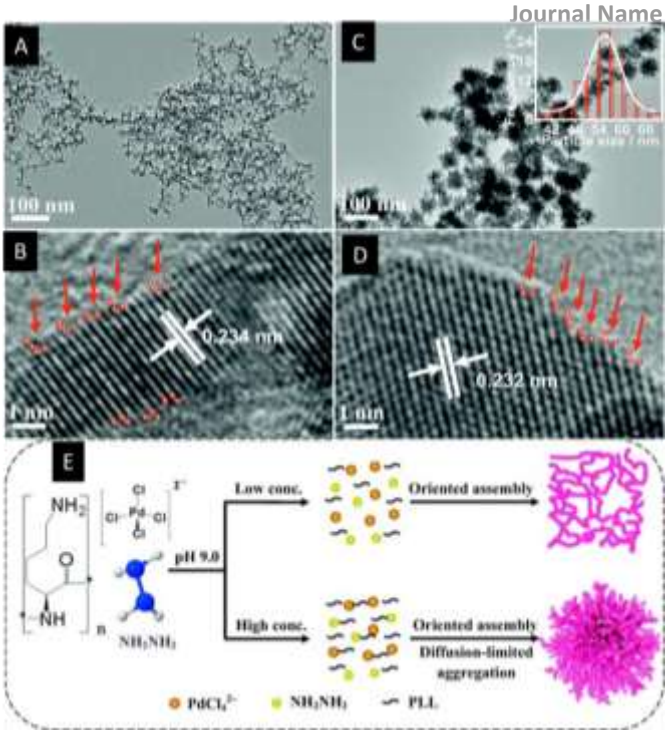


**Fig. 14**. (A) and (B) TEM and HRTEM images of Pd nanowires; (C) and (D) TEM and HRTEM images of dendrite-like Pd nanoparticles obtained at higher PLL conc. (E) The proposed formation mechanism of Pd NCNs and Pd NDs via surfactant based self-assembly. Reproduced with permission.[89] Copyright 2018 Elsevier.

concentration of PLL, the length of Pd nanochains decreases,

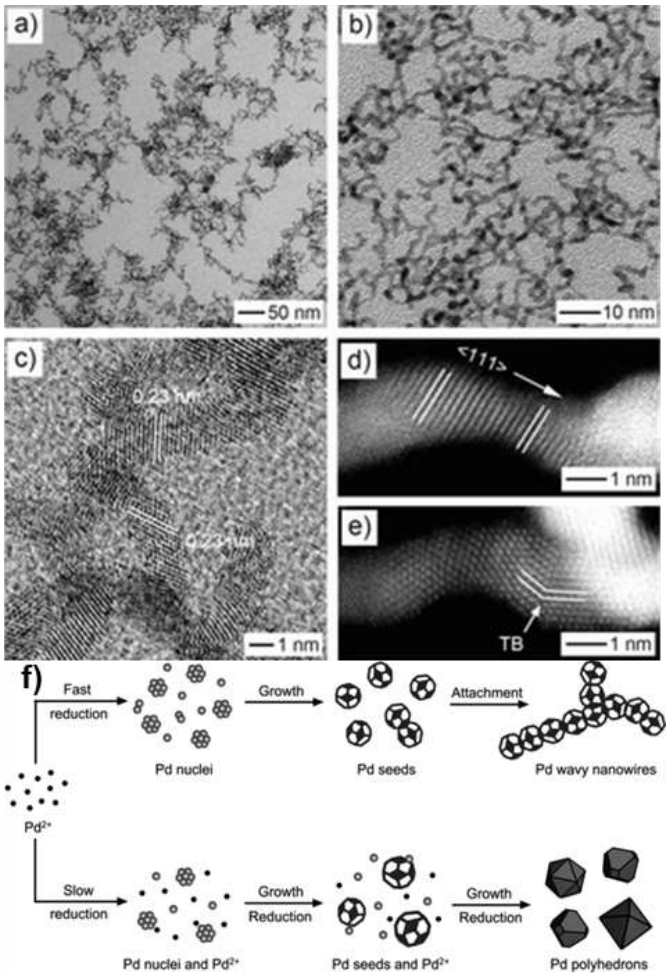


**Fig. 15** a,b) TEM images of a typical sample of Pd nanowires prepared by polyol synthesis. c) HR BF-STEM image of the Pd nanowires; d,e) HR HAADF-STEM images of a Pd nanowire highlighting the twin boundary (TB); f) A schematic illustration of the effects of reaction kinetics on Pd nanowire formation . Reproduced with permission.[8] Copyright 2013 Wiley-VCH.

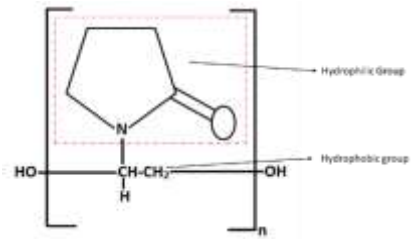


**Fig.16** Structure of PVP

resulting in agglomerated dendritic structures as seen in Fig. 14 C and D. PLL has a strong chelating ability; the amino groups on PLL coordinate with Pd to form a complex (PLL-$PdCl_4^{2-}$) which is later reduced by hydrazine to Pd atoms in nanoparticles covered with excess PLL. These freshly prepared Pd nanoparticles possess high surface energy and quickly become faceted, exposing {111} crystal planes with the lowest energy[85] and fuse to form nanochain networks, directed by hydrogen bonds formed by PLL in water (Fig. 14 E).

Unlike NWs with high aspect ratio, wavy or worm-like NWs are made using a different strategy. Wang et al.[8] reported the synthesis of ultrathin palladium NWs by a polyol method relying on the oriented attachment growth process. Two separate solutions of diethylene glycol, one containing PVP as a capping agent and the other containing $(CF_3COO)_2Pd$ were prepared. The solution containing Pd salt was quickly injected into the PVP-DEG solution at 140 °C. The reaction was stopped after 3 hours, and the particles were collected, washed, and re-dispersed in DI water. TEM showed NWs 2±0.6 nm in width and several tens to hundreds of nm in length. Similar results were obtained when the Pd salt precursor was changed to $(CH_3COO)_2Pd$. However, with $PdCl_4^{2-}$, Pd polyhedra were obtained. A TEM imaging study of the nanoparticles at various time intervals suggested that initial reduction of the salt precursor led to a burst of thermodynamically unstable Pd seeds. The high-energy facets collided and fused to minimize total surface energy and produce Pd NWs enclosed with lower-energy {111} facets. The high-resolution bright-field scanning transmission electron microscopy (BF-STEM) image in Fig. 15 c shows lattice fringes with a spacing of 0.23 nm corresponding to (111) planes. Furthermore, high-resolution high-angle annular dark-field STEM (HAADF-STEM) images of the sample (Fig. 15 d, e) reveal that either single-crystal structure or twin-boundaries (TB) are formed by coalescence of Pd seeds at high-energy facets. These observations led the authors to suggest a possible mechanism of NW formation *via* oriented attachment. They concluded that a nucleation burst of nanoparticles from Pd precursors with fast reaction kinetics and low surface charge on particles facilitated van der Waals force-driven attachment and led to the formation of NWs as summarized in Fig. 15 f.

#### Factors affecting palladium NWs synthesis

**Effect of capping agents.** The most common capping agent used for 1D Pd nanostructures is PVP. Thus, here we mainly limit our discussion to the effect of PVP on Pd morphology. PVP is a non-toxic and non-ionic polymer with C=O, C-N, and $CH_2$ functional groups. PVP has a strong hydrophilic component (the pyrrolidone moiety) and a hydrophobic component (the alkyl groups). Because of its highly polar amide group, PVP dissolves very well in polar solvents like water, ethanol, EG, etc. Its hydrophobic backbone can play a role in preventing particle aggregation. PVP also acts as a mild reducing agent because of the hydroxyl group it possesses at the ends of its chain.[90 91] When used in colloidal synthesis, PVP can attach to the facets with higher energy to reduce the overall surface energy of the nanoparticles, and thus also acts as a structure-directing agent. Because of all the advantages it provides, PVP is widely used in shape-controlled synthesis of noble metal nanocrystals.

PVP promotes NW formation by binding to higher energy facets (100) of Pd nanocrystals, which leaves the lower energy (111) facets for new Pd atoms to attach and continue growing. Several studies have considered the effect of PVP concentration on Pd NW formation. Huang et al.[46] observed that when the concentration of PVP in the solution was halved, relative to the optimal concentration for NW growth, Pd particles with mixed morphologies were obtained. On the other hand, doubling the concentration of PVP led to the formation of spheres and NRs. Lim et al.[86] observed that the molecular weight of PVP also affected the yield of Pd NWs. They were able to obtain a higher yield of Pd NWs using PVP55 (with molecular weight of ~55000) than with PVP29 (with molecular weight of ~29000) which gave a mixture of NWs and nanoparticles. Xiong et al.[91] reported a similar observation that the conversion of $Na_2PdCl_4$ decreased with in increasing molecular weight of PVP. Higher molecular weight PVP results in slower reduction kinetics, which is essential for NW formation.

Apart from PVP, various other surfactants like CTAB,[52,92–95] DODAC,[11,64,88] and oleylamine,[96,97] have been used to synthesize Pd-based NWs and NRs.

**Effect of addition of halide ion.** Zhang et al.[98] reported the synthesis of Pd NWs using a chemical reduction method with $NaBH_4$ as a reducing agent and PVP/KI as structure directing agents. They reported the dual role of bromide not only in promoting NW formation, but also in determining the diameter of NWs. The classical formula for the critical radius of nuclei is given as:

$$r = \frac{4\gamma M}{\rho RT \ln \frac{a(r)}{a}} \quad (1)$$

Where $r$ is the nuclei critical size, $\gamma$ is surface tension of the nucleus-solvent interface, $M$ is the molar mass, $\rho$ is density, $T$ is absolute temperature, $R$ is the gas constant, and $a$ is the material activity. In this model, the critical radius is directly proportional to surface tension. When halide ions attach to the surface of Pd nuclei, the surface tension decreases, which in turn leads to a decrease of critical radius of Pd NWs. Attachment of bromide ions can be regulated by adjusting the pH of the solution, and weaker adsorption of bromide can lead to a higher growth rate. At a given, limited, Pd concentration,

higher growth rate can lead to structural defects which, in turn, can affect the electrocatalytic performance of Pd NWs.

Similarly, Wang et al.[10] investigated the importance of bromide ions ($Br^-$) in the synthesis of trimetallic PtPdCu NWs and found that aggregates were formed instead of alloy nanochain networks with uniform composition when the reaction was carried out without KBr. Hong et al.[82] reported similar observations for PdAu NW networks using chemical reduction of Pd and Au salt solutions by $NaBH_4$ with PVP and KBr as capping agents. They found that without KBr, small particles were obtained, while synthesis carried out with excess KBr resulted in aggregated nanostructures. Bromide ion is believed to slow the reduction rate by forming $[PdBr_4]^{2-}$ and $[AuBr_4]^-$ complexes. Bromide ions also specifically bind onto (100) facets, while leaving lower energy (111) facets available for new atoms to attach and grow into 1D structures.

Apart from Pd-based nanochain and NW networks, the effect of the addition of halide ions on high aspect ratio Pd NWs was also investigated by several researchers. Huang et al.[44] reported that NaI assisted in the synthesis of Pd NWs by the polyol method. They investigated the effect of halide ions on the reduction kinetics of Pd(II) using UV-vis analysis to measure the concentration of Pd(II) precursor throughout the reaction. They observed that replacing $I^-$ with $Br^-$ resulted in polyhedra instead of NWs. To study the reaction kinetics and effect of halide ions, characteristic absorbances of $PdI_4^{2-}$ (408 nm) and $PdBr_4^{2-}$ (332 nm) were used to track the concentration of Pd(II) ions in both standard synthesis and modified synthesis. They obtained rate constants for each case by plotting the integrated form of a first-order reaction rate law:

$$\ln[A]_t = -kt + \ln[A]_0 \quad (2)$$

where $[A]_t$ and $[A]_0$ denote time-dependent and initial concentrations of Pd(II) precursor, respectively; $t$ is time, and $k$ is the rate constant. The rate constant with $Br^-$ was more than 2 orders of magnitude faster than for the original synthesis using $I^-$.

**Effect of pH.** pH control is very important for solution phase synthesis of NWs. Some synthesis methods require basic conditions for NW formation,[80 10 61] while others require acidic conditions.[99 44 100 92] Lan et al.,[79] discovered that the pH of the solution played an important role in synthesis. Pd nanochains were synthesized only when the solution pH was near 7. When the reaction was carried out at pH 2, particle-like morphology was observed, which was due to electrostatic repulsion of the protonated carboxylic groups of PVP. At higher pH (>10), the nanochains tend to form highly aggregated masses due to precipitation of $PdCl_4^{2-}$ and a decrease in solubility of PVP at higher pH. They also observed that Pd nanochains prepared at pH 7 demonstrated the best electrocatalytic activity. In the synthesis of palladium NRs, Tang et al.[100] observed that pH was directly correlated with the length of Pd NRs formed, which increased with the addition of HCl. They found that when the amount of 1M HCl used in their synthesis was increased from 10µL to 120µL, while keeping other reaction conditions fixed, the average length of NRs increased from ~100 to ~500 nm

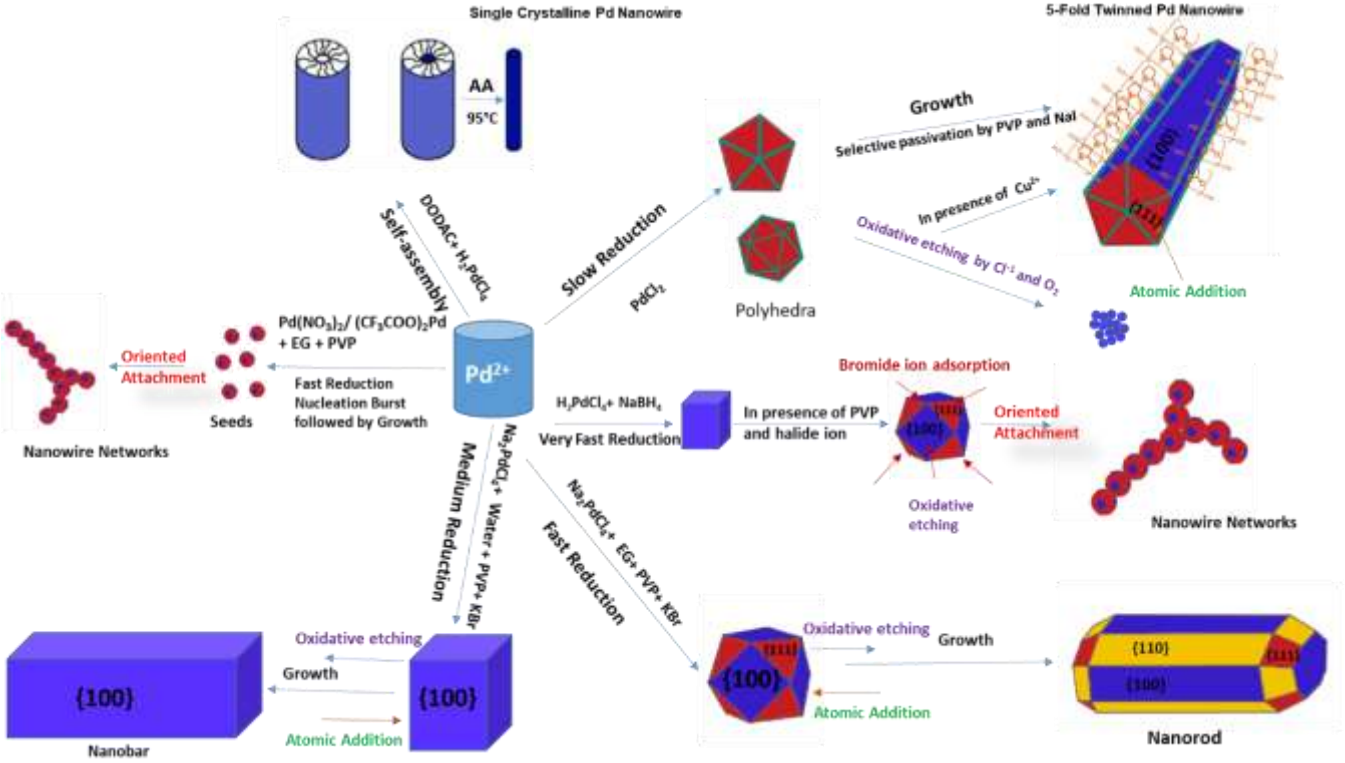


**Fig. 17** Summary of solution phase synthesis of 1D Pd nanostructures and factors affecting it.

while their diameter remained constant.

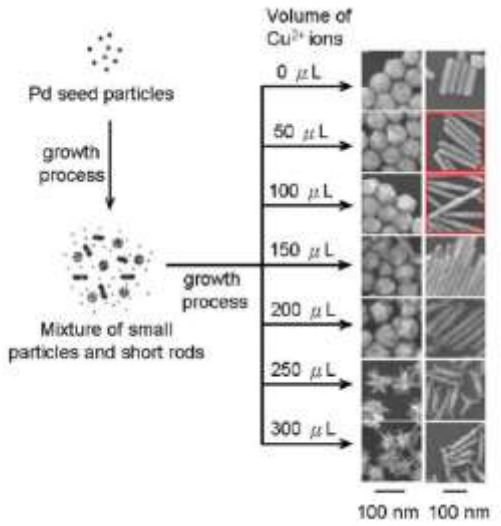


**Fig. 18** The growth process of palladium nanocrystals and the final products obtained with the addition of different amounts of $Cu^{2+}$ ions. Reproduced with permission.[53] Copyright 2009 American Chemical Society

Zhang et al.[98] reported that surface roughness of Pd NWs in their synthesis method was directly related to the pH of the system. They prepared Pd NWs of different diameters using a wet chemical reduction method with PVP and KBr as capping agents and $NaBH_4$ as their reducing agent. They carried out the reaction at different pH values, and generally observed that the NW diameter decreased with decreasing pH. However, above pH 11, the NW diameter decreased with increasing pH. Thus, the maximum NW diameter was obtained at pH 11.

**Effect of sacrificial oxidation on palladium NWs.** Oxidative etching is the removal of zerovalent atoms of metals as solvated ions by oxidative species like dissolved $O_2$, chloride ions, or Fe(III)/Fe(II).[101] Such etching is often viewed as an undesirable phenomenon that breaks Pd twinned seeds into single crystal seeds by etching at twin planes, or that dissolves nuclei back into solution. However, localized oxidative etching can also be used intentionally to remove twinned seeds and generate single crystal nanobars and NRs. In work done by Xiong et al.,[38] localized oxidative etching on one specific surface was used to initiate preferential growth on that face and obtain Pd nanobars and NRs. Effects of oxidative etching are summarized in Fig 17.

Huang et al.[44] reported that when their reaction proceeded for a longer time, all the Pd NWs were converted into tadpole-like structures. They also suggested that the presence of NaI and HCl was the cause for instability of penta-twinned structures. Iodide ions contribute to oxidative etching by forming a $PdI_4^{2-}$ complex according to the following equation:

$$Pd + O_2 + 4I^- + 4H^+ \rightarrow PdI_4^{2-} + 2H_2O \quad (3)$$

The role of oxygen in destabilizing Pd NWs is clear from the above equation. To study the effect of oxidative etching, they carried out reactions at 150 °C and found that the rate of oxidative etching slowed down as compared to the standard procedure.

There are several means of avoiding oxidative etching. Introducing a foreign species, such as a trace amount of Cu or Ag salt[100] can remove oxygen, which preferentially reacts with Cu or Ag rather than Pd, and enhances the formation of penta-twinned structures. Lu et al.[47] demonstrated the use of small organic molecules (acetonitrile, acetone, 1,4-dioxane, 1,3,5-trioxane) to tune oxidative etching to achieve a high yield of 5-fold twinned Pd NWs.

Tang et al.[100] also investigated the effect of sacrificial oxidation of Ag and Cu ions on Pd NR formation. They observed that the amount of 1D nanostructures obtained was less than 5% if the amount of $AgNO_3$ added was reduced from the standard concentration. To further understand the role of $AgNO_3$ in NR formation, they observed that the best results were obtained only when Ag was added during the nucleation stage. When they replaced Ag(I) with Cu(II), similar results were obtained, although the NRs were shorter. They hypothesized that Ag and Cu ions are reduced first and later serve as templates for twinned structures of Pd, which evolve into Pd NRs later.

Lim et al.[86] were able to use a trace amount of copper salt to synthesize palladium NWs in high yield by hydrothermal synthesis. Because PVP is a weak reducing agent that cannot reduce $Cu^{2+}$ ions by itself, they suggested that Cu promoted the growth of Pd NWs by acting as a sacrificial target for oxidation by the trace amount of $O_2$ dissolved in water. In the absence of $Cu^{2+}$ ions, this dissolved $O_2$, along with chloride ions, caused oxidative etching of Pd crystal seeds back into solution. Penta-twinned Pd seeds are preferentially etched, which suppresses NW growth. They hypothesized that $Cu^{2+}$ ions form CuI complexes with excess iodide in the system and are later oxidized to CuO by oxygen present in water.

Chen et al.[53] demonstrated a seed-mediated synthesis of palladium NRs through the addition of copper acetate salt into the growth solution. Pd NRs of different dimensions were obtained by adding different volumes of Cu salt solution, as shown in Fig. 18. The synthesis was carried out in two steps, where a seed solution of Pd nanoparticles and small NRs was synthesized first using CTAB as surfactant and AA as reducing agent. This seed solution was later combined with varying volumes of $Cu(OAc)_2$ solutions to produce Pd NRs of different dimensions. They observed that the length of Pd NRs increased with increasing volume of Cu salt solution added. Increasing the volume of Cu salt solution by more than 4 times led to the formation of branched Pd nanostructures. To further investigate the role of Cu in the growth of NRs, they replaced $Cu(OAc)_2$ with $Cu(NO_3)_2$, $CuSO_4$, and $CuCl_2$ and found that Pd morphology did not depend on the source of Cu; similar results were obtained in each case. However, replacing the Cu salt with the same amount of a salt of another transition metal, such as $Ni(OAc)_2$, $Zn(OAc)_2$ or $AgNO_3$, did not produce Pd NRs. Instead, Pd polyhedra were obtained in each case. They hypothesized that because Cu has a reduction potential that is very close to, but slightly smaller than, that of Pd it can assist in the growth of Pd NRs by first being reduced to create nucleation or deposition sites, then re-oxidized and removed from the final structure.

## Applications

### Catalytic Applications

**Electrochemical oxidation of methanol, ethanol, formic acid, and ethylene glycol.** Direct liquid fuel cells have gained attraction as promising clean, environmentally friendly and portable energy sources. These fuel cells operate by the oxidation of small organic molecules such as methanol, ethanol, or formic acid at the negative electrode (anode). [3,102] Pt-based catalysts are the most widely used materials in this application, but due to some limitations such as their high price, limited world supply and low oxidation rates, other alternatives have been proposed in recent years. Palladium is considered a possible replacement for platinum with potentially superior performance.[103] However, developing highly efficient, stable, and economically feasible electrocatalysts based on palladium remains a major challenge. Electrocatalytic performance depends on the morphology, composition and surface structure of the catalyst.[42] Electrochemical applications of various palladium-based nanomaterials have been discussed thoroughly in another review paper.[3] In this section, 1D Pd-based nanomaterials for the electro oxidation of formic acid, methanol, ethanol, and ethylene glycol are specifically considered.

Pd electrocatalysts containing 1-D nanostructures including Pd NW networks,[104] nanochains,[105] NWs,[63] and nanochain networks[89] have been reported for electro-oxidation of formic acid. Tang et al.[100] reported higher electrocatalytic activity of Pd NRs compared to nanocubes. In addition, they showed a decrease in formic acid oxidation activity with increase in the NR length. The activity enhancement with length reduction may come from faults at the interfaces of (111) facets. Wang et al.[8] reported a catalytic current density 2.5 times higher than the conventional Pd/C catalysts by introducing ultrathin Pd wavy NWs with diameters of 2 nm. The higher activity of these NWs was attributed to their unique wavy, wire-like structure and the inclusion of numerous twin defects. Recently, Ding et al. [7] introduced a high-performance bifunctional electrocatalyst for formic acid and formate oxidation (in acidic and alkaline media) using freestanding mesoporosity-decorated palladium NT arrays (P-PdNTAs). The nanomaterials provide a high electrochemically active surface area with a high density of catalytically active sites per unit area. The P-PdNTA showed a gravimetric catalytic current of 3.65 A $mg^{-1}$ at ≈0.3 V versus Saturated Calomel Electrode (SCE) for formic acid oxidation, 8.5 times higher than commercial Pt/C.

Another solution to increase the activity and stability of the Pd-based 1D nanomaterials is to introduce other elements in their structure. Nanomaterials that have been investigated include Pt-decorated coral-like Pd nanochain networks,[79] PdBi NWs,[96] PdP nanoparticle networks,[61] PdSn nanochain networks,[106] trimetallic PtPdCu NWs,[10] AuPd alloyed NW networks,[80] PdCu and PtPdCu NWs,[107] and twisted PdCu nanochains.[108] Du et al.[109] prepared PdNi porous alloy NWs by chemical dealloying of Ni. They attributed the higher activity and improved durability of PdNi NWs to the modification of electronic structure of Pd by Ni that facilitated the removal of poisoning intermediates on Pd. Lu et al.[42] reported the formic acid electro-oxidation activity of PdAg NWs. The charge transfer resistance ($R_{CT}$) of formic acid oxidation on PdAg NWs was smaller than conventional Pd/C catalysts suggesting that the electron-transfer kinetics for formic acid oxidation were highly facilitated. In addition, the PdAg NWs displayed higher CO tolerance and more negative onset potential, probably due to the synergistic effects of Pd and Ag in the NW. Bin et al.[110] presented the enhanced catalytic oxidation of formic acid using PdNi NW networks supported on reduced graphene oxide (RGO). They suggested a Pd:Ni molar ratio of 1:1 as the optimum composition. The mass-normalized forward peak current density of the PdNi/RGO was up to 604.3 mA $mg^{-1}$, 4.63 times higher than that of commercial Pd/C. The enhanced electrocatalytic performance of the PdNi/RGO probably could be attributed to the fact that with the addition of Ni, the nickel hydroxide species on the surface of the NW networks generate OH species to facilitate the oxidative desorption of the intermediate products and regenerate the Pd active sites.

A few papers reported the catalytic activity of trimetallic Pd-based NWs for methanol electro-oxidation.[10 111] Guo et al.[112] investigated the activity of ultralong Pt-on-Pd bimetallic NWs with Pd NW cores and dendritic Pt shells for methanol electro-oxidation. Compared to the commercial *E*-TEK catalyst, a significant enhancement of the peak current and a negative shift of the onset potential for methanol oxidation was observed. They suggested that the multi-dimensional nanostructures with abundant interconnected nanobranches could provide facile pathways for electron transfer by reducing the interface resistance between nanobranches. Zhu et al.[72] demonstrated the enhanced catalytic activity of PdPt and PdAu alloy NWs for ethanol, methanol, and glucose electro-oxidation in an alkaline medium. $Pd_{45}Pt_{55}$ showed the highest activity for ethanol and methanol electro-oxidation and its mass activity was also higher than single metallic Pd or Pt NWs. They reported the high electrocatalytic activity of PdAu alloy NWs for glucose oxidation, which exceeded that of previously reported nanomaterials such as Pt–Pb NW arrays, palladium nanoparticle-single walled carbon NT hybrid nanostructures, porous gold, and mesoporous platinum. Recently, Wang et al.[113] reported synthesis of PdCo NWs with a jagged appearance for methanol electro-oxidation. Benefiting from cobalt doping as well as jagged structure, the mass and specific activities of PdCo NWs were ~3.2 times and ~2.1 times higher than those of Pd/C catalysts, respectively. Also, the NWs showed lower susceptibility to CO poisoning and higher stability.

Compared to methanol, ethanol has lower toxicity and higher theoretical energy density (8.1 kWh $kg^{-1}$ for ethanol vs 6.1 kWh $kg^{-1}$ for methanol) and thus has attracted attention in direct liquid fuel cell applications.[3] Hong et al.[82] reported a highly active PdAu NW network as a self-supported electrocatalyst for ethanol electro-oxidation. The addition of Au on Pd may improve the adsorption of $OH_{ads}$ onto the surface of the catalyst and thus activate the catalyst surface

and enhance the ethanol oxidation process. Zhao et al.[114] found an optimum composition of PdCu branched networks for ethanol electro-oxidation. $Pd_{73}Cu_{27}$ exhibited a 178% enhancement in Pd-based mass activity, 160% improvement in long-term stability and better tolerance against poisoning by CO-like species compared with a commercial Pd/C catalyst. The oxidative removal of reaction intermediates ($CH_3CO_{ad}$ and $CO_{ad}$) adsorbed on Pd surfaces determines the overall oxidation current. Incorporation of Cu weakens the adsorption of oxygenated intermediates on the Pd surface. However, at higher Cu content, the adsorption strength of intermediates on the PdCu surface is too low to activate the adsorbed intermediate, which reduced the activity. In a similar paper, Liu et al.[115] reported $Pd_{80}$-$Cu_{20}$ nanochain networks as the optimum composition for ethanol oxidation. Begum et al.[95] introduced bifunctional palladium nanonetworks for both ethanol oxidation and hydrogen evolution reactions. They compared the activity of Pd nanonetworks with PdZn nanonetworks and Pd nanoparticles. Among these catalysts, they reported the highest mass activity of 2.04 A $mgPd^{-1}$ for Pd nanonetworks for the peak of the forward scan of the Cyclic Voltammetry (CV) curve. This current was 3.5 times that of Pt/C electrocatalysts. Lv et al.[88] introduced noble metal-phosphorus alloy NWs for ethanol electro-oxidation. They developed ternary PdCuP alloy NWs with enhanced mass activity of 6.7 A $mg_{Pd}^{-1}$, 9.4 fold higher than commercial Pd nanoparticle catalysts. Alloying Pd alloyed with a metal (Cu) or non-metal (P) could weaken the adsorption of the intermediates ($CO_{ads}$ and $CH_3CO_{ads}$) by modifying the electronic states of Pd, and also optimize the further removal/oxidation of poisoning intermediates by promoting the formation of $OH_{ads}$ (Cu-$OH_{ads}$ and P-$OH_{ads}$) (Fig 19a). Fig. 19 b, shows the measured electrochemically active surface areas (ECSAs) of all the nanocatalysts, obtained from oxygen desorption peaks of cyclic voltammograms (CVs) in 1.0 M KOH. Among all the nanomaterials, PdCuP NWs showed the highest ECSA (Fig. 19 c). Fig. 19 d shows the CVs in 1.0 M KOH and 1.0 M ethanol, indicating all above nanocatalysts are electrocatalytically active for the ethanol oxidation reaction. The values are compared in Fig. 19 e. The same research group, in another study, presented the activity of PdAg single crystalline NWs for ethanol electro-oxidation.[11]

Several groups have applied 1D Pd-based nanomaterials for ethylene glycol electro-oxidation. Materials considered include worm-like Pd NTs,[116] PdTe NWs,[73] PdAu NW networks,[117] and PdCu alloy NWs.[50] Hong et al.[118] used bimetallic PtPd NW networks for ethylene glycol and glycerol oxidation. The NWs exhibited different activities at different compositions with $Pd_{55}Pt_{30}$ being optimal. None of the PdPt NW networks showed a significant decrease in catalytic activity after an extended stability test, while the commercial Pt/C only retained about 50% of its initial catalytic activity under the same testing conditions. They attributed this high activity and stability to the modified electronic states and synergistic effects between Pd and Pt.

**Electrochemical reduction of Oxygen.** In addition to electrocatalysts for fuel oxidation at the anode, there is a need to boost the performance of electrocatalysts for oxygen reduction reaction (ORR) at the cathode of a fuel cell. Sluggish oxygen reduction kinetics as well as the high cost and low stability of Pt are key impediments to the commercialization of fuel cells.[98] Pd alloys in the form of NWs and NRs have been introduced as alternatives to Pt nanomaterials. Koenigsmann et al.[119] reported a series of Pd-based NWs including $Pd_{1-x}Au_x$, $Pd_{1-x}Pt_x$ and Pt~$Pd_9Au$ NWs. The enhanced activity of NWs compared to nanoparticles has been attributed to a size-induced contraction of the NW surface, resulting in an advantageous change in the electronic properties of the NW. In another study, PtPd nanomaterials were tested in the form of porous NRs. Because of the high specific surface area, unique one-dimensional morphology, and alloy structure, the porous PtPd NRs exhibited superior electrocatalytic activity toward the ORR *via* an efficient $4e^-$ pathway.[120] Moreover, there are some reports on active platinum-free nanomaterials for the ORR.[49] For instance, Liu et al.[121] presented efficient ultrathin PdNi nanostructures and highlighted the "volcano"-type relationship between chemical composition and corresponding ORR activity. $Pd_{0.90}Ni_{0.10}$ was the optimum composition for the prepared NWs. In contrast, for nanoparticles, $Pd_{0.60}Ni_{0.40}$ was found to be the best combination. The authors suggested that significant differences in the surface structure and strain of the NWs and nanoparticles may lead to differing degrees of surface segregation at the catalytic interface. The surface layers of the $Pd_{0.60}Ni_{0.40}$ nanoparticles and of $Pd_{0.90}Ni_{0.10}$ NWs likely possess approximately the same chemical composition at the interface and, therefore, a similar "active site" profile.

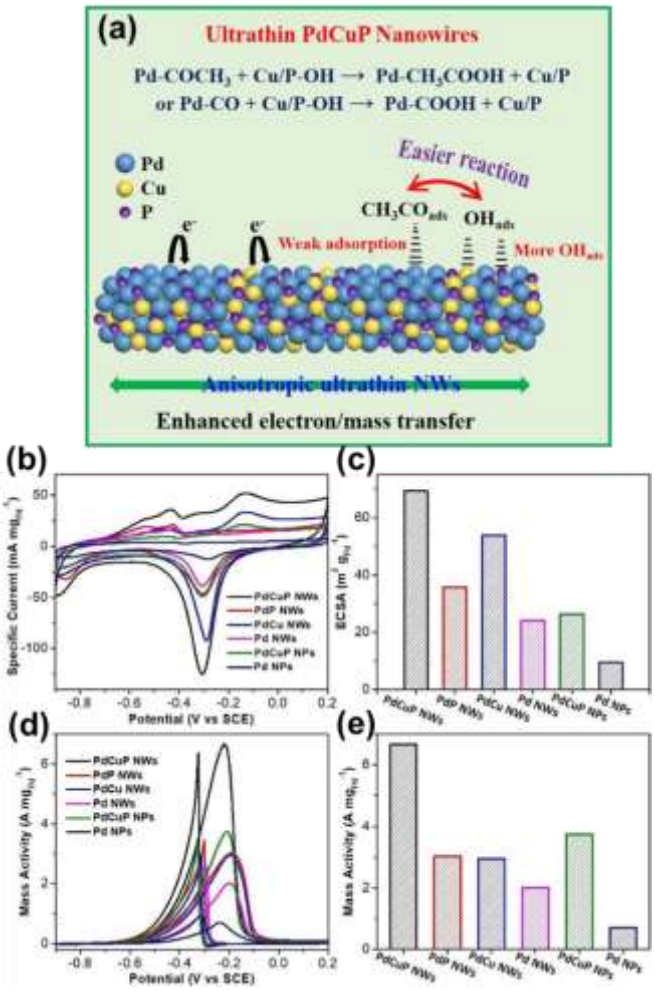


**Fig. 19** a) Schematic illustrating the electrocatalytic ethanol electro-oxidation on ultrathin ternary PdCuP alloy nanowires; b) CV curves and c) summarized ECSAs of ultrathin PdCuP, PdP, PdCu, and Pd NWs, PdCuP NPs, and commercial Pd NPs in 1.0 M KOH. d) CV curves and e) summarized mass activities of ultrathin PdCuP, PdP, PdCu, and Pd NWs, PdCuP NPs, and commercial Pd NPs in 1.0 M KOH and 1.0 M ethanol. Reproduced with permission.[89] Copyright 2019 Elsevier.

**Electrochemical evolution of hydrogen.** Recently, interest has grown in using palladium-based NWs for water-splitting and especially its half reaction, the hydrogen evolution reaction (HER).[97] Lv et al.[64] reported anisotropic single-crystalline ultra-long PdPt nanostructures with high activity and stability for the HER. The 1-D structure provided more exposed active sites, easier electron transfer, and high utilization efficiency on crystal surfaces for the HER. Yang et al.[122] investigated the performance of PdIr NWs on reduced graphene oxide for both the hydrogen evolution and oxygen evolution reactions. They believe PdIr NWs not only exhibit the inherent catalytic activities of elemental Pd and Ir, but also provide efficient transport pathways for electrons.

**Cross Coupling Reactions.** Palladium-catalyzed cross-coupling reactions are selective and convenient routes for reacting an organometallic compound with an organic halide under mild conditions to form a new carbon-carbon bond in the organic product.[123] Unlike other shapes of palladium-based nanoparticles, only a few papers reported the application of 1-D palladium nanomaterials for reactions such as the Suzuki, Heck, and Sonogashira reactions. Palladium-tellurium alloy NRs were used in the Heck reactions.[123] Chen et al.[53] first reported the catalytic activity of palladium NRs and branched nanocrystals for a Suzuki coupling reaction between phenylboronic acid and iodobenzene. NRs with length of ~300

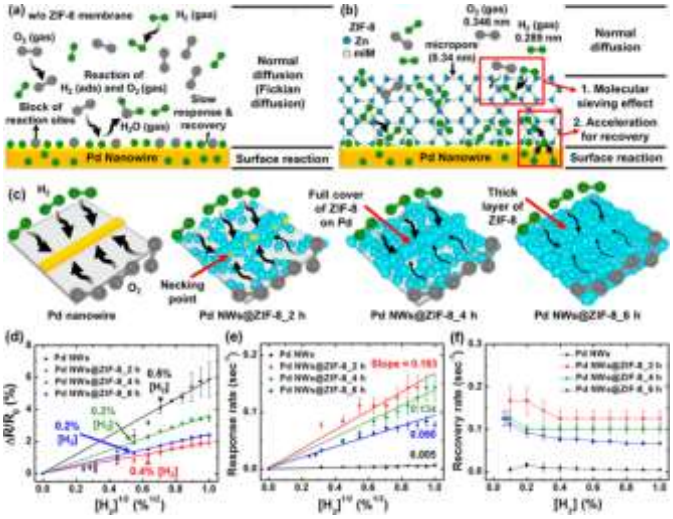


**Fig. 20** Schematic illustration of Pd NWs@ZIF-8 hydrogen sensor. a) Sensing model for Pd NWs without ZIF-8 membrane, and (b) sensing model for Pd NWs@ZIF-8. Without ZIF-8, $H_2$ sensing can be significantly affected by oxygen in air. In the presence of ZIF-8, $O_2$ diffusion is limited. (c) Fabrication of Pd@ZIF-8 at different time interval; Pd NW, Pd NWs@ZIF-8_2 h, Pd NWs@ZIF-8_4 h, and Pd NWs@ZIF-8_6 h. (d) Response *vs* $[H_2]^{0.5}$ in air, (e) response rate *vs* $[H_2]^{0.5}$ in air, and (f) recovery rate *versus* $[H_2]$. Reproduced with permission.[25] Copyright 2017 American Chemical Society.

nm performed slightly better than branched nanocrystals. Li et al.[33] grew palladium NRs in the mesoporous channels of SBA-15 and reported the yield of Suzuki coupling reaction between 4-bromotoluene and phenylboronic acid, which was much higher than palladium nanoparticles on SBA-15. In addition, the palladium NR/SBA-15 samples were more durable compared to the palladium nanoparticle/SBA-15. Nadagouda et al.[124] studied the catalytic activity of palladium nanobelts, nanoplates, and nanotrees for C–C bond forming reactions under microwave irradiation. Li et al.[125] addressed the challenge of the separation and reusability of palladium-based nanocatalysts for Suzuki coupling. They prepared Pd NW arrays in the pores of anodic aluminum oxide templates. Less than 0.1% Pd loss was reported after five cycles, and leaching of the catalysts into the reaction mixture was not observed.

### Hydrogen Sensors

Global warming and rising fossil fuel prices have driven a search for alternative clean sources of energy. A hydrogen-based economy can contribute to meeting energy needs while minimizing impact on the environment.[4] The combustion of hydrogen with oxygen only produces water ($H_2O$) as a byproduct, thus making it a promising clean fuel.[25] With its potential to be used as an automobile fuel in the future, there is a need for fast, reliable, cheap and compact hydrogen sensors to detect hydrogen even at very low concentration. Although numerous hydrogen sensors are commercially available, substantial research is still continuing, aiming to improve selectivity, response time, and reliability of hydrogen sensors while making them smaller and less expensive.[5]

Because of the high selectivity of palladium towards absorbing hydrogen, it has been widely studied as a hydrogen sensing material. This feature, coupled with the high surface-to-volume ratio of palladium NWs makes them an excellent candidate for developing fast and accurate hydrogen sensors.[126] The hydrogen sensing behaviour of Pd NWs can be described as follows: It starts with adsorption of $H_2$ molecules on the surface of Pd, this is followed by dissociation of $H_2$ into H atoms. The H atoms diffuse through the Pd fcc lattice and form palladium hydride ($PdH_x$). This insertion of H atoms into the Pd lattice causes expansion of their lattice which in turn causes an increase in electrical resistance.[21] This volume expansion of Pd NWs increases linearly with increasing H concentration. Pd has α and β phases that result from $H_2$ adsorption below 293°C. The β phase has slightly larger lattice constant and increased hydrogen solubility.[127] The α-β phase transformation causes irreversible deformation of the Pd lattice and produces hysteresis in the response to $H_2$, which decreases the stability and reliability of Pd NW-based sensors. One possible means of suppressing the α-β phase transformation is by alloying Pd with other metals like Au, Ag, and Cu.[128] So far hydrogen sensors based on pure Pd NWs[14,16,134,135,25,78,126,129–133], and Pd-based alloy NWs[21,24,36,37,136–138] have been tested. The following section summarizes these studies.

**Pure palladium NW-based hydrogen sensors.** Bulk Pd-based hydrogen sensors suffer from limitations including large internal stress, buckling of films, and slow response because of long diffusion pathways for hydrogen. Most of these problems can be solved using single Pd NW-based sensors.[135] Various methods have been developed to synthesize single palladium NW-based hydrogen sensors. The most common strategies for Pd NW synthesis for this application are the physical methods discussed in the first part of this review. Specific examples of fabrication of Pd NWs and their use as hydrogen sensors are summarized below.

Offermans at al.[20] used a technique that they call "deposition and etching under angles" to fabricate an array of single palladium NWs. The Pd NWs fabricated using this strategy had diameters between 50-80 nm and lengths of approximately 7 µm. The sensor could detect $H_2$ concentrations as low as 27 ppm with a response time varying from a few seconds to just below a minute. The observed that bias voltage had an effect on response time, and by changing it from 50 to 800 mV, they were able to reduce the response time from 12 s to 4s for 2.4% $H_2$ in $N_2$. In the same year, Yang et al.[130] investigated the effect of diameter of single palladium NWs on hydrogen detection. They fabricated two Pd NWs of different diameters: one with diameter 5 nm (named nc5), and the other with diameter of 15 nm (nc15). They observed a correlation between Pd NW diameter and their behaviour upon exposure to $H_2$. nc5 suffered fracture on exposure to $H_2$, whereas nc15 was able to resist fracture while rapidly and reversibly detecting hydrogen down to 2 ppm at room temperature. They later studied the effect of Pd NW dimensions on sensitivity (defined as $\Delta R/R_{air} \times 100\%$) and concluded that smaller NWs have slightly enhanced sensitivity, but they could not determine the reason behind it. They also found that Pd NWs exhibit faster response and recovery compared to Pd films. They proposed that response and recovery rates for Pd NW-based hydrogen sensors are always directly proportional to their surface area/volume ratio and hence smaller NWs make faster hydrogen sensors than larger NWs. However, Pd NW fabrication using microfabrication techniques is costly. Most of the Pd NW sensors have been tested with a mixture of $H_2$ in $N_2$, whereas a real hydrogen sensor has to work in air. The $O_2$ present in air is known to interfere with detection of hydrogen, often causing low sensitivity and slow response/recovery time. The same group recently accelerated the response time of Pd NWs in air by taking advantage of the nanofiltration ability of zeolite imidazole framework (ZIF-8). They discovered that sensing properties of their palladium NW based hydrogen sensor improved drastically when a layer of ZIF-8 was grown over the Pd NW sensor. ZIF-8 acted as a filter preventing larger molecules of $O_2$ from coming in contact with Pd NWs while allowing $H_2$ to pass through it (Fig 20).[25]

Most of the single Pd NW-based hydrogen sensors require a cleanroom environment and sophisticated fabrication strategy, which raises the cost of Pd-based hydrogen sensors. Many researchers have been looking for cost effective ways to make Pd NWs for hydrogen sensors. In this effort, Hinai et al.[134] reported synthesis of ultra-sensitive $H_2$ sensors using DNA-templated Pd NWs. The hydrogen sensor showed great sensitivity to low concentrations of $H_2$, demonstrating the promise of this method for creating low cost sensors. Zheng et al.[135] fabricated a low cost hydrogen sensor using commercial filtration membranes. The fabrication method they used could

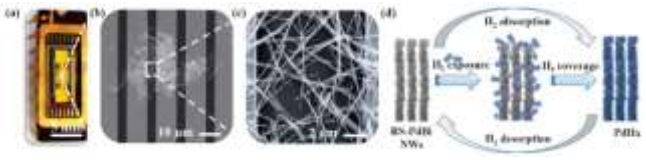

**Fig. 21** (a) Hydrogen sensor prototype. (b, c) Sequentially magnified SEM images of the interdigitated electrode integrated with multiple rough-surface (RS)-PdBi NWs. (d) Schematic illustration of the RS-PdBi NWs for $H_2$ adsorption and desorption cycles. Reproduced with permission.[21] Copyright 2019 American Chemical Society.

be extended to Pd alloy and other hydrogen sensing materials. Beyond those already discussed, many innovative techniques have been used to fabricate flexible and robust hydrogen sensors using Pd NW membranes. Lim et al.[78] developed a wet chemical process for synthesis of Pd NT arrays to be used as flexible hydrogen sensors. The Pd NT arrays were prepared by a galvanic displacement reaction of ZnO NW arrays grown on flexible substrates. Interconnected Pd NTs with high surface area provided high sensitivity. A year later, Lim et al.[131] used nanoimprint lithography to fabricate a flexible palladium hydrogen sensor. The flexible sensor could detect $H_2$ gas concentrations as low as 50 ppm with a response time of 57 s.

**Palladium alloy NW hydrogen sensor.** Using palladium alloy NWs instead of pure palladium NWs for hydrogen sensing has several advantages. First, palladium is currently the costliest of all noble metals (Kitco Gold Index, June 10, 2019) and alloying it with other metals would bring down the cost of

manufacturing. Second, when Pd is alloyed with other metals like Au, Ir, or Pt, it can become more sensitive to hydrogen, as hydrogen can penetrate deeper due to expansion of the crystal lattice.[139,140] Third, alloying Pd with other metals like Ag and Cu eliminates hydrogen embrittlement of Pd NWs and is known to supress α-β phase transitions in Pd.[136,141]

Yang et al.[36] fabricated a Pd-Cu superlattice NW array-based hydrogen sensor that displayed faster response times and recovery times, by factors of ~9 and ~7 times, compared to palladium NW-based sensors without Cu NW layers. A year later, Fang et al.[142] reported a bi-dimensional alumina-palladium NW-based hydrogen sensor using inner channels of porous alumina. The fabricated hydrogen sensor displayed high sensitivity and was able to reliably detect as little as 0.1% $H_2$ in air with a short response time of 1s for 1% $H_2$ in air. Jang et al.[136] reported synthesis of a transparent hydrogen sensor using hollow Pd-Ag composite NWs. The hollow Pd@Ag NWs were synthesized by galvanic replacement of LPNE-patterned Ag NWs with palladium. Au NWs were further laid perpendicular to Pd@Ag NWs and the final device was demonstrated as a flexible wearable hydrogen sensor. Because the hollow tubular structures provide a larger area for $H_2$ to contact, the fabricated detector showed reversible and repetitive detection of 900 ppm of $H_2$ gas. Cho et al. [137] reported a Pt functionalized PdO-based hydrogen sensor which displayed superior $H_2$ sensitivity of 62% as compared to just 6.1% achieved with a pure PdO NW-based hydrogen sensor, due to dissociation of $H_2$ on the Pt surface. The sensor could detect $H_2$ down to 10 ppm with a sensitivity of 14%. In a more recent work, a hydrogen sensor based on PdBi NWs was demonstrated by Du et al.[21] PdBi NWs with rough surfaces was prepared by chemical etching of PdBi NWs obtained from electrodeposition on an AAO template (Fig. 21). The fabricated hydrogen sensor displayed reliable and repeatable performance over a wide temperature range (160-400K) owing to synergistic effects of Pd and Bi in NWs with optimal Bi content of 15 at.% .

#### Biochemical sensors

NW structures are preferred for biosensing applications because of their high surface-to-volume ratio, good electrical conductivity, and enhanced catalytic capability. Recently, bimetallic alloy nanostructures have garnered much attention for electrochemical sensing applications. Bimetallic alloy NW-based sensors are more stable and take advantage of the synergistic effects of catalytic activity and conductivity of the metal NWs. Ye et al.[143] reported a Pd-Au based electro-chemiluminescence biosensor for detection of acetylcholinesterase (AChE). A year later, Song et al.[144] developed a Pd-Cu NW network-based electrochemical biosensor for organophosphate pesticide (OP) detection in fruits and vegetables using immobilized AChE. The sensor was based on inhibition of AChE in contact with OPs; this leads to a decrease in activity that can be detected in terms of reduced current. The Pd-Cu NWs not only provided up to 3.8 times more surface area for immobilization of AChE as compared to bare glass carbon electrode but also displayed remarkable electron mobility as well as electro-catalytic activity. More recently, Pd@Au NR-,[145] and Pd@Au NW network-[99] based biosensors were also developed for OP detection. These showed remarkable stability and high accuracy in real sample analysis. Apart from OPs, palladium NTs synthesized using CdS modified AAO templates were shown to be a promising material for nonenzymatic glucose sensors.[146]

#### Hydrogen storage

Palladium is known to absorb large volumetric quantities of hydrogen at room temperature and atmospheric pressure. When hydrogen comes in contact with palladium, it forms $PdH_x$ and occupies interstitial octahedral sites of the fcc cubic lattice.[4] Because of its ability to store a large volume of hydrogen and because of the large surface-to-volume ratio of Pd NWs, several studies have explored their $H_2$ gas storage capacity. Gilbert et al.[147] reported the synthesis of palladium NW foams using cross-linking and freeze-drying and studied their hydrogen gas storage capacity. Pd NWs (200 nm in diameter and 15 μm in length) were synthesized using electrodeposition into porous templates and were later dispersed in water and sonicated to produce a uniform dispersion. The sonicated Pd NW slurry was immediately frozen, then placed in vacuum for 12 hours to sublime the interstitial ice. The hydrogen storage capacity of the NW foam was found to reach a H:Pd ratio of 0.61, which is comparable to the H:Pd ratio of bulk Pd.

Several studies have shown that palladium-based alloys have greater hydrogen solubility and storage capacity than pure Pd. Adams et al.[148] reported an increase in hydrogen sorption by up to 15 times in Pd nanostructures containing 10-15% Cd, compared to nanoporous Pd networks. They attributed the enhanced $H_2$ sorption to the increased lattice constant, dendritic structure, and decrease in crystallite size of Pd-Cd nanostructures. Lu et al.[149] reported that PdAg NTs (15% Pd) prepared by galvanic displacement reaction of Ag NWs displayed enhanced hydrogen storage ability over 200 times that pure Pd nanoparticles. They speculated that the high storage capacity of their nanomaterials was probably due to their tubular structure. In more recent work, Namba et al. [139] reported that Pd with a monolayer of gold shows enhanced hydrogen sorption by a factor of more than 40. They realized that the rate-limiting step in hydrogen sorption is penetration of hydrogen to the subsurface of bulk Pd. The presence of a monolayer of Au on the Pd surface leads to lattice expansion of Pd so that hydrogen can penetrate deeper which results in higher solubility of H in Pd-Au alloys. Similar results were presented by Kobayashi et al.,[140] who reported doubling of the hydrogen storage capacity of $Pd_{0.8}Ir_{0.2}$ core (Pd) /shell (Ir) nanoparticles compared to bulk Pd.

## Conclusion and Outlook

This review has detailed and compared the evolution of Pd NWs both in terms of synthesis methods and applications that

have been carried over the past two decades. Physical methods of Pd NW synthesis have been explored widely to fabricate individual NWs (LNPE, EBIB, and electrochemical deposition) or arrays of NWs or NTs using hard templates. Chemical methods of Pd-based NW synthesis have come a long way in the last two decades, and different morphologies like nanochain or NW networks, wormlike, twisted, or penta-twinned NWs have been synthesized in good yield. The growth mechanisms of these anisotropic nanostructures are not entirely understood, but recent development of new analytical and computational tools may provide more insight and understanding of the underlying mechanisms. *In situ* TEM, though not yet applied to Pd NW synthesis, may provide information about the growth of Pd seeds from solution and their self-assembly into 1D NWs. A few studies have considered the growth of Pd seeds, the kinetics of growth, and phase changes in $H_2$-containing atmospheres.[150–153] However, *in situ* TEM of Pd-based NWs could provide further insight into their formation mechanism. Computational tools like density functional theory (DFT) and molecular simulations can improve understanding of the mechanisms of Pd-based NW formation. DFT, in particular, has been used to understand preferential attachment of PVP to Ag surfaces while acting as structure directing agent.[154,155] Although, a few DFT studies of Pd NW applications have been published,[156,157] such studies need to be extended to address synthesis of Pd-based NWs, including the preferential attachment of not only PVP but other agents such as halide ions. Improving understanding of the mechanisms of Pd-based NW formation can help in future scaling of these synthesis methods from current mg level production to grams and kg.

With the skyrocketing price of palladium, there has been a surge in research to reduce the use of Pd while increasing its performance in particular applications. One possible solution is to use Pd nanomaterials with more active facets. In many applications, the unique morphology of Pd NWs bounded by {111} facets has proven to be advantageous over bulk Pd or 0D Pd nanostructures. Another possible approach is to alloy Pd with other metals (Au, Pt, Cu, Bi, Ir, Ce) and non-metals (P) to reduce cost while maintaining the same or better performance. In many cases, doping Pd with certain metals at an optimum composition has improved performance relative to bulk Pd, with reduced catalytic poisoning. Furthermore, combining Pd-based NWs with support materials like silica, carbon, and metal-organic frameworks (MOFs) can enhance their stability towards harsh reaction conditions. Owing to these observations, the last few years have seen a surge in publications exploring the synergistic effects of incorporating various elements into Pd NWs for applications ranging from electrocatalysis to hydrogen storage and sensing. With no indication that the price of Pd will fall in the coming years, the area of Pd-based NW synthesis and applications needs more emphasis on optimization of bimetallic and trimetallic NW compositions and uniform distribution of Pd NWs on supports, which can reduce Pd requirements in applications.

Several advances in solution phase synthesis of palladium-based NWs have been reviewed in this paper. However, there are some inherent limitations of this route that must be addressed if this method is to become a commercial success. Solution phase synthesis of Pd-based NWs usually requires a large quantity of solvent and produces a similar quantity of solvent waste at the end of synthesis. For large-scale production of Pd-based NWs at low cost, this issue must be addressed. One possible solution is to explore greener synthesis methods employing bio-based templates and less toxic chemicals. Another major issue with solution-processed NWs is that of surface capping agents attached to the surface of NWs. Complete removal of PVP or halide ions attached to the surface of Pd NWs can be extremely difficult, and if left on the NW surface they often lower the catalytic activity or other performance measures in applications. Currently, post-synthesis cleaning with methods like ozone treatment, plasma treatment, acetic acid, or strong base treatment are used to eliminate surface passivating agents. More work needs to be done in the post-synthesis treatment of nanoparticles and liquid waste reduction for Pd-based NWs.

With the effects of climate change becoming more adverse year by year, energy systems based on carbon-free hydrogen as an energy carrier may be a viable option for replacing fossil fuels. Palladium-based NWs can play an important role in this shift toward a hydrogen economy due to their excellent electrocatalytic and hydrogen sorption abilities. In this review, we have summarized the performance of Pd-based NWs for hydrogen production, storage, and detection. The primary issue faced in hydrogen sorption by Pd NWs is that of hydrogen embrittlement. Although much progress has been made using Pd alloy NWs instead of pure Pd NWs, which is known to suppress the α-β phase transition, inconsistencies in terms of reproducibility and replicability of results remain, and require more attention during the coming years to boost the role of Pd-based NWs in the hydrogen economy.

## Conflicts of interest

There are no conflicts to declare.

## Acknowledgements

This work is supported in part by the U.S. Department of Energy, Office of Fossil Energy, under Award Number DE-FE0026463 and by the National Science Foundation, grant number CBET-1804996.

## Notes and references

1 J. Hu, T. W. Odom and C. M. Lieber, *Acc. Chem. Res.*, 1999, **32**, 435–445.
2 S. Kar and S. Chaudhuri, *Synth. React. Inorganic, Met. Nano-Metal Chem.*, 2006, **36**, 289–312.
3 A. Chen and C. Ostrom, *Chem. Rev.*, 2015, **115**, 11999–12044.
4 B. D. Adams and A. Chen, *Mater. Today*, 2011, **14**, 282–289.

5 T. Hübert, L. Boon-Brett, G. Black and U. Banach, *Sensors Actuators B Chem.*, 2011, **157**, 329–352.
6 L. Ma, D. Chu and R. Chen, *Int. J. Hydrogen Energy*, 2012, **37**, 11185–11194.
7 J. Ding, Z. Liu, X. Liu, J. Liu, Y. Deng, X. Han, C. Zhong and W. Hu, *Adv. Energy Mater.*, 2019, 1900955.
8 Y. Wang, S. Il Choi, X. Zhao, S. Xie, H. C. Peng, M. Chi, C. Z. Huang and Y. Xia, *Adv. Funct. Mater.*, 2014, **24**, 131–139.
9 M. Iqbal, Y. V. Kaneti, J. Kim, B. Yuliarto, Y. M. Kang, Y. Bando, Y. Sugahara and Y. Yamauchi, *Small*, 2019, **15**, 1804378.
10 P. Wang, Y. Zhang, R. Shi and Z. Wang, *New J. Chem.*, 2018, **42**, 19083–19089.
11 H. Lv, Y. Wang, A. Lopes, D. Xu and B. Liu, *Appl. Catal. B Environ.*, 2019, **249**, 116–125.
12 Y. Xiong and Y. Xia, *Adv. Mater.*, 2007, **19**, 3385–3391.
13 J. Yang, Y. Ji, Q. Shao, N. Zhang, Y. Li and X. Huang, *Adv. Funct. Mater.*, 2018, **28**, 1803722.
14 Y. Im, C. Lee, R. P. Vasquez, M. A. Bangar, N. V. Myung, E. J. Menke, R. M. Penner and M. Yun, *Small*, 2006, **2**, 356–358.
15 T. Bhuvana and G. U. Kulkarni, *ACS Nano*, 2008, **2**, 457–462.
16 M. Cho, J. Zhu, H. Kim, K. Kang and I. Park, *ACS Appl. Mater. Interfaces*, 2019, **11**, 13343–13349.
17 E. C. Walter, M. P. Zach, F. Favier, B. J. Murray, K. Inazu, J. C. Hemminger and R. M. Penner, *ChemPhysChem*, 2003, **4**, 131–138.
18 S. J. Jeong and S. O. Kim, *J. Mater. Chem.*, 2011, **21**, 5856–5859.
19 A. Enrico, V. Dubois, F. Niklaus and G. Stemme, *ACS Appl. Mater. Interfaces*, 2019, **11**, 8217–8226.
20 P. Offermans, H. D. Tong, C. J. M. Van Rijn, P. Merken, S. H. Brongersma and M. Crego-Calama, *Appl. Phys. Lett.*, 2009, **94**, 223110.
21 L. Du, L. Zheng, H. Wei, S. Zheng, Z. Zhu, J. Chen and D. Yang, *ACS Appl. Nano Mater.*, 2019, **2**, 1178–1184.
22 C. Xiang, M. A. Thompson, F. Yang, E. J. Menke, L. M. C. Yang and R. M. Penner, *Phys. Status Solidi Curr. Top. Solid State Phys.*, 2008, **5**, 3503–3505.
23 C. Xiang, S. C. Kung, D. K. Taggart, F. Yang, M. A. Thompson, A. G. Güell, Y. Yang and R. M. Penner, *ACS Nano*, 2008, **2**, 1939–1949.
24 X. Li, Y. Liu, J. C. Hemminger and R. M. Penner, *ACS Nano*, 2015, **9**, 3215–3225.
25 W. T. Koo, S. Qiao, A. F. Ogata, G. Jha, J. S. Jang, V. T. Chen, I. D. Kim and R. M. Penner, *ACS Nano*, 2017, **11**, 9276–9285.
26 E. C. Walter, K. Ng, M. P. Zach, R. M. Penner and F. Favier, *Microelectron. Eng.*, 2002, **61–62**, 555–561.
27 L. Xiao, L. Zhuang, Y. Liu, J. Lu and H. D. Abruña, *J. Am. Chem. Soc.*, 2009, **131**, 602–608.
28 F. Yang, D. K. Taggart and R. M. Penner, *Nano Lett.*, 2009, **9**, 2177–2182.
29 A. K. Das, N. H. Kim, D. Pradhan, D. Hui and J. H. Lee, *Compos. Part B Eng.*, 2018, **144**, 11–18.
30 K.-B. Lee, S.-M. Lee and J. Cheon, *Adv. Mater.*, 2001, **13**, 517–520.
31 D. Wang, W. L. Zhou, B. F. McCaughy, J. E. Hampsey, X. Ji, Y. B. Jiang, H. Xu, J. Tang, R. H. Schmehl, C. O'Connor, C. J. Brinker and Y. Lu, *Adv. Mater.*, 2003, **15**, 130–133.
32 A. Fukuoka, H. Araki, Y. Sakamoto, S. Inagaki, Y. Fukushima and M. Ichikawa, *Inorganica Chim. Acta*, 2003, **350**, 371–378.
33 J. Li, X. Bai and H. Lv, *Microporous Mesoporous Mater.*, 2019, **275**, 69–75.
34 K. Kim, M. Kim and S. M. Cho, *Mater. Chem. Phys.*, 2006, **96**, 278–282.
35 C. Xu, H. Wang, P. K. Shen and S. P. Jiang, *Adv. Mater.*, 2007, **19**, 4256–4259.
36 D. Yang, J. Carpena-Núñez, L. F. Fonseca, A. Biaggi-Labiosa and G. W. Hunter, *Sci. Rep.*, 2014, **4**, 3773.
37 W. Wang, X. Liu, S. Mei, Y. Jia, M. Liu, X. Xue and D. Yang, *Sensors Actuators, B Chem.*, 2019, **287**, 157–164.
38 Y. Xiong, H. Cai, B. J. Wiley, J. Wang, M. J. Kim and Y. Xia, *J. Am. Chem. Soc.*, 2007, **129**, 3665–3675.
39 S. Cheong, J. D. Watt and R. D. Tilley, *Nanoscale*, 2010, **2**, 2045–2053.
40 H. Zhang, M. Jin, Y. Xiong, B. Lim and Y. Xia, *Acc. Chem. Res.*, 2013, **46**, 1783–1794.
41 H. Dong, Y. C. Chen and C. Feldmann, *Green Chem.*, 2015, **17**, 4107–4132.
42 Y. Lu and W. Chen, *ACS Catal.*, 2012, **2**, 84–90.
43 Q. Shi, C. Zhu, C. Bi, H. Xia, M. H. Engelhard, D. Du and Y. Lin, *J. Mater. Chem. A*, 2017, **5**, 23952–23959.
44 H. Huang, A. Ruditskiy, S. Il Choi, L. Zhang, J. Liu, Z. Ye and Y. Xia, *ACS Appl. Mater. Interfaces*, 2017, **9**, 31203–31212.
45 S. Feng and R. Xu, *Acc. Chem. Res.*, 2001, **34**, 239–247.
46 X. Huang and N. Zheng, *J. Am. Chem. Soc.*, 2009, **131**, 4602–4603.
47 N. Lu, W. Chen, G. Fang, B. Chen, K. Yang, Y. Yang, Z. Wang, S. Huang and Y. Li, *Chem. Mater.*, 2014, **26**, 2453–2459.
48 T. Yang, Y. Ma, Q. Huang, G. Cao, S. Wan, N. Li, H. Zhao, X. Sun and F. Yin, *Electrochem. commun.*, 2015, **59**, 95–99.
49 T. Yang, Y. Ma, Q. Huang and G. Cao, *Nano Energy*, 2016, **19**, 257–268.
50 B. Yan, H. Xu, K. Zhang, S. Li, J. Wang, Y. Shi and Y. Du, *Appl. Surf. Sci.*, 2018, **434**, 701–710.
51 A. Gole and C. J. Murphy, *Chem. Mater.*, 2004, **16**, 3633–3640.
52 G. Berhault, M. Bausach, L. Bisson, L. Becerra, C. Thomazeau and D. Uzio, *J. Phys. Chem. C*, 2007, **111**, 5915–5925.
53 Y. H. Chen, H. H. Hung and M. H. Huang, *J. Am. Chem. Soc.*, 2009, **131**, 9114–9121.
54 H. Huang, L. Zhang, T. Lv, A. Ruditskiy, J. Liu, Z. Ye and Y. Xia, *ChemNanoMat*, 2015, **1**, 246–252.
55 S. Gao, H. Zhang, X. Wang, W. Mai, C. Peng and L. Ge, *Nanotechnology*, 2005, **16**, 1234–1237.
56 Y. Xia, P. Yang, Y. Sun, Y. Wu, B. Mayers, B. Gates, Y. Yin, F. Kim and H. Yan, *Adv. Mater.*, 2003, **15**, 353–389.
57 F. Ksar, G. Surendran, L. Ramos, B. Keita, L. Nadjo, E. Prouzet, P. Beaunier, A. Hagège, F. Audonnet and H. Remita, *Chem. Mater.*, 2009, **21**, 1612–1617.
58 C. Jiang, S. Ranjit, Z. Duan, Y. L. Zhong, K. P. Loh, C. Zhang

and X. Liu, *Nanoscale*, 2009, **1**, 391–394.
59 P. F. Siril, A. Lehoux, L. Ramos, P. Beaunier and H. Remita, *New J. Chem.*, 2012, **36**, 2135–2139.
60 Y. Imura, K. Tsujimoto, C. Morita and T. Kawai, *Langmuir*, 2014, **30**, 5026–5030.
61 J. Zhang, Y. Xu and B. Zhang, *Chem. Commun.*, 2014, **50**, 13451–13453.
62 X. Gao, F. Lu, W. Yang, F. Shang and L. Zheng, *RSC Adv.*, 2016, **6**, 67495–67501.
63 D. Xu, X. Liu, M. Han and J. Bao, *Chem. Commun.*, 2016, **52**, 12996–12999.
64 H. Lv, X. Chen, D. Xu, Y. Hu, H. Zheng, S. L. Suib and B. Liu, *Appl. Catal. B Environ.*, 2018, **238**, 525–532.
65 T. Kijima, T. Yoshimura, M. Uota, T. Ikeda, D. Fujikawa, S. Mouri and S. Uoyama, *Angew. Chemie - Int. Ed.*, 2003, **43**, 228–232.
66 M. Chawla, R. Kumar and P. F. Siril, *J. Mol. Catal. A Chem.*, 2016, **423**, 126–134.
67 J. Richter, R. Seidel, R. Kirsch, M. Mertig, W. Pompe, J. Plaschke and H. K. Schackert, *Adv. Mater.*, 2000, **12**, 507–510.
68 K. Nguyen, M. Monteverde, A. Filoramo, L. Goux-Capes, S. Lyonnais, P. Jegou, P. Viel, M. Goffman and J.-P. Bourgoin, *Adv. Mater.*, 2008, **20**, 1099–1104.
69 S. Kundu, K. Wang, D. Huitink and H. Liang, *Langmuir*, 2009, **25**, 10146–10152.
70 X. Chen, J. Wang, T. Odoom-Wubah, X. Jing, J. Huang, Q. Li and Y. Zheng, *Mater. Lett.*, 2016, **165**, 29–32.
71 L. Hai-Wei, L. Shuo, G. Jun-Yan, W. Shang-Bing, W. Lei and Y. Shu-Hong, *Adv. Mater.*, 2009, **21**, 1850–1854.
72 C. Zhu, S. Guo and S. Dong, *Adv. Mater.*, 2012, **24**, 2326–2331.
73 W. Hong, J. Wang and E. Wang, *CrystEngComm*, 2015, **17**, 9011–9015.
74 L. Sahoo, M. Rana, S. Mondal, N. Mittal, P. Nandi, A. Gloskovskii, U. Manju, D. Topwal and U. K. Gautam, *Nanoscale*, 2018, **10**, 21396–21405.
75 Z. Li, H. Lu, Q. Li, X. S. Zhao and P. Guo, *Colloids Surfaces A Physicochem. Eng. Asp.*, 2015, **464**, 129–133.
76 S. M. Alia, K. Duong, T. Liu, K. Jensen and Y. Yan, *ChemSusChem*, 2014, **7**, 1739–1744.
77 S. M. Kim, L. Liu, S. H. Cho, H. Y. Jang and S. Park, *J. Mater. Chem. A*, 2013, **1**, 15252–15257.
78 M. A. Lim, D. H. Kim, C. O. Park, Y. W. Lee, S. W. Han, Z. Li, R. S. Williams and I. Park, *ACS Nano*, 2012, **6**, 598–608.
79 F. Lan, D. Wang, S. Lu, J. Zhang, D. Liang, S. Peng, Y. Liu and Y. Xiang, *J. Mater. Chem. A*, 2013, **1**, 1548–1552.
80 T. Yuan, H. Y. Chen, X. Ma, J. J. Feng, P. X. Yuan and A. J. Wang, *J. Colloid Interface Sci.*, 2018, **513**, 324–330.
81 J. Wang, Y. Chen, H. Liu, R. Li and X. Sun, *Electrochem. commun.*, 2010, **12**, 219–222.
82 W. Hong, J. Wang and E. Wang, *ACS Appl. Mater. Interfaces*, 2014, **6**, 9481–9487.
83 F. Li, Y. Ji, S. Wang, S. Li and Y. Chen, *Electrochim. Acta*, 2015, **176**, 125–129.
84 Y. Xia, X. Xia and H.-C. Peng, *J. Am. Chem. Soc.*, 2015, **137**, 7947–66.
85 J. M. Zhang, F. Ma and K. W. Xu, *Appl. Surf. Sci.*, 2004, **229**, 34–42.
86 M. B. Lim, J. L. Hanson, L. Vandsburger, P. B. Roder, X. Zhou, B. E. Smith, F. S. Ohuchi and P. J. Pauzauskie, *J. Mater. Chem. A*, 2018, **6**, 5644–5651.
87 J. Reyes-Gasga, J. L. Elechiguerra, C. Liu, A. Camacho-Bragado, J. M. Montejano-Carrizales and M. J. Yacaman, *J. Cryst. Growth*, 2006, **286**, 162–172.
88 H. Lv, L. Sun, D. Xu, Y. Ma and B. Liu, *Appl. Catal. B Environ.*, 2019, **253**, 271–277.
89 X. F. Zhang, Y. Chen, L. Zhang, A. J. Wang, L. J. Wu, Z. G. Wang and J. J. Feng, *J. Colloid Interface Sci.*, 2018, **516**, 325–331.
90 K. M. Koczkur, S. Mourdikoudis, L. Polavarapu and S. E. Skrabalak, *Dalt. Trans.*, 2015, **44**, 17883–17905.
91 Y. Xiong, I. Washio, J. Chen, H. Cai, Z. Y. Li and Y. Xia, *Langmuir*, 2006, **22**, 8563–8570.
92 H. M. Song and J. I. Zink, *Langmuir*, 2018, **34**, 4271–4281.
93 S. I. Park and H.-M. Song, *Chem. Lett.*, 2019, **48**, 277–280.
94 L. Xu, K. Wang, B. Jiang, W. Chen, F. Liu, H. Hao, C. Zou, Y. Yang and S. Huang, *Chem. Mater.*, 2016, **28**, 7394–7403.
95 H. Begum, M. S. Ahmed and S. Jeon, *ACS Appl. Mater. Interfaces*, 2017, **9**, 39303–39311.
96 H. Liao, J. Zhu and Y. Hou, *Nanoscale*, 2014, **6**, 1049–1055.
97 S. C. Lim, C. Y. Chan, K. T. Chen and H. Y. Tuan, *Nanoscale*, 2019, **11**, 8518–8527.
98 Y. L. Zhang, X. L. Sui, L. Zhao, D. M. Gu, G. S. Huang and Z. B. Wang, *Int. J. Hydrogen Energy*, 2019, **44**, 6551–6559.
99 X. Lu, L. Tao, Y. Li, H. Huang and F. Gao, *Sensors Actuators, B Chem.*, 2019, **284**, 103–109.
100 Y. Tang, R. E. Edelmann and S. Zou, *Nanoscale*, 2014, **6**, 5630–5633.
101 R. Long, S. Zhou, B. J. Wiley and Y. Xiong, *Chem. Soc. Rev.*, 2014, **43**, 6288–6310.
102 C. Bianchini and P. K. Shen, *Chem. Rev.*, 2009, **109**, 4183–4206.
103 E. Antolini, *Energy Environ. Sci.*, 2009, **2**, 915.
104 S. Wang, X. Wang and S. P. Jiang, *Nanotechnology*, , DOI:10.1088/0957-4484/19/45/455602.
105 J. N. Zheng, M. Zhang, F. F. Li, S. S. Li, A. J. Wang and J. J. Feng, *Electrochim. Acta*, 2014, **130**, 446–452.
106 Y. Gong, X. Liu, Y. Gong, D. Wu, B. Xu, L. Bi, L. Y. Zhang and X. S. Zhao, *J. Colloid Interface Sci.*, 2018, **530**, 189–195.
107 H. Liu, R. R. Adzic and S. S. Wong, *ACS Appl. Mater. Interfaces*, 2015, **7**, 26145–26157.
108 L. Y. Zhang, Y. Gong, D. Wu, G. Wu, B. Xu, L. Bi, W. Yuan and Z. Cui, *J. Colloid Interface Sci.*, 2019, **537**, 366–374.
109 C. Du, M. Chen, W. Wang and G. Yin, *ACS Appl. Mater. Interfaces*, 2011, **3**, 105–109.
110 D. Bin, B. Yang, F. Ren, K. Zhang, P. Yang and Y. Du, *J. Mater. Chem. A*, 2015, **3**, 14001–14006.
111 C. Shang, Y. Guo and E. Wang, *Nano Res.*, 2018, **11**, 4348–4355.
112 S. Guo, S. Dong and E. Wang, *Chem. Commun.*, 2010, **46**, 1869–1871.
113 C. Wang, L. Zheng, R. Chang, L. Du, C. Zhu, D. Geng and D. Yang, *ACS Appl. Mater. Interfaces*, 2018, **10**, 29965–29971.

114 X. Zhao, J. Zhang, L. Wang, Z. Liu and W. Chen, *J. Mater. Chem. A*, 2014, **2**, 20933–20938.
115 J. Liu, Z. Huang, K. Cai, H. Zhang, Z. Lu, T. Li, Y. Zuo and H. Han, *Chem. - A Eur. J.*, 2015, **21**, 17779–17785.
116 J. J. Feng, D. L. Zhou, H. X. Xi, J. R. Chen and A. J. Wang, *Nanoscale*, 2013, **5**, 6754–6757.
117 H. Xu, B. Yan, K. Zhang, C. Wang, J. Zhong, S. Li, Y. Du and P. Yang, *Colloids Surfaces A Physicochem. Eng. Asp.*, 2017, **522**, 335–345.
118 W. Hong, C. Shang, J. Wang and E. Wang, *Energy Environ. Sci.*, 2015, **8**, 2910–2915.
119 C. Koenigsmann, E. Sutter, T. A. Chiesa, R. R. Adzic and S. S. Wong, *Highly enhanced electrocatalytic oxygen reduction performance observed in bimetallic palladium-based nanowires prepared under ambient, surfactantless conditions*, 2012, vol. 12.
120 Y. Lu, Y. Jiang and W. Chen, *Nano Energy*, 2013, **2**, 836–844.
121 H. Liu, C. Koenigsmann, R. R. Adzic and S. S. Wong, *ACS Catal.*, 2014, **4**, 2544–2555.
122 A. Yang, T. Li, S. Jiang, X. Wang, X. Qiu, W. Lei and Y. Tang, *Nanoscale*, , DOI:10.1039/C9NR03027A.
123 A. Bej, K. Ghosh, A. Sarkar and D. W. Knight, *RSC Adv.*, 2016, **6**, 11446–11453.
124 M. N. Nadagouda, V. Polshettiwar and R. S. Varma, *J. Mater. Chem.*, 2009, **19**, 2026.
125 R. Li, P. Zhang, Y. Huang, C. Chen and Q. Chen, *ACS Appl. Mater. Interfaces*, 2013, **5**, 12695–12700.
126 D. Yang, L. Valentín, J. Carpena, W. Otaño, O. Resto and L. F. Fonseca, *Small*, 2013, **9**, 188–192.
127 M. Fisser, R. A. Badcock, P. D. Teal and A. Hunze, *Sensors Actuators B Chem.*, 2018, **259**, 10–19.
128 F. Gu, H. Zeng, Y. B. Zhu, Q. Yang, L. K. Ang and S. Zhuang, *Adv. Opt. Mater.*, 2014, **2**, 189–196.
129 E. C. Walter, F. Favier and R. M. Penner, *Anal. Chem.*, 2002, **74**, 1546–1553.
130 F. Yang, D. K. Taggart and R. M. Penner, *Nano Lett.*, 2009, **9**, 2177–2182.
131 S. H. Lim, B. Radha, J. Y. Chan, M. S. M. Saifullah, G. U. Kulkarni and G. W. Ho, *ACS Appl. Mater. Interfaces*, 2013, **5**, 7274–7281.
132 F. Yang, S. C. Kung, M. Cheng, J. C. Hemminger and R. M. Penner, *ACS Nano*, 2010, **4**, 5233–5244.
133 M. N. Al-Hinai, R. Hassanien, N. G. Wright, A. B. Horsfall, A. Houlton and B. R. Horrocks, *Faraday Discuss.*, 2013, **164**, 71–91.
134 M. Al Hinai, N. Wright, A. Horsfall, R. Hassanien, B. Horrocks and A. Houlton, in *Proceedings of IEEE Sensors*, IEEE, 2011, pp. 1–4.
135 X. Q. Zeng, M. L. Latimer, Z. L. Xiao, S. Panuganti, U. Welp, W. K. Kwok and T. Xu, *Nano Lett.*, 2011, **11**, 262–268.
136 J. S. Jang, S. Qiao, S. J. Choi, G. Jha, A. F. Ogata, W. T. Koo, D. H. Kim, I. D. Kim and R. M. Penner, *ACS Appl. Mater. Interfaces*, 2017, **9**, 39464–39474.
137 H. J. Cho, V. T. Chen, S. Qiao, W. T. Koo, R. M. Penner and I. D. Kim, *ACS Sensors*, 2018, **3**, 2152–2158.
138 C. Fournier, K. Rajoua, M. L. Doublet and F. Favier, *ACS Appl. Mater. Interfaces*, 2013, **5**, 310–318.
139 K. Namba, S. Ogura, S. Ohno, W. Di, K. Kato, M. Wilde, I. Pletikosić, P. Pervan, M. Milun and K. Fukutani, *Proc. Natl. Acad. Sci.*, 2018, **115**, 7896–7900.
140 H. Kobayashi, M. Yamauchi, R. Ikeda, T. Yamamoto, S. Matsumura and H. Kitagawa, *Chem. Sci.*, 2018, **9**, 5536–5540.
141 N. A. Al-Mufachi, N. V. Rees and R. Steinberger-Wilkens, *Renew. Sustain. Energy Rev.*, 2015, **47**, 540–551.
142 J. Fang, I. Levchenko, X. Lu, D. Mariotti and K. Ostrikov, *Int. J. Hydrogen Energy*, 2015, **40**, 6165–6172.
143 C. Ye, M. Q. Wang, X. Zhong, S. Chen, Y. Chai and R. Yuan, *Biosens. Bioelectron.*, 2016, **79**, 34–40.
144 D. Song, Y. Li, X. Lu, M. Sun, H. Liu, G. Yu and F. Gao, *Anal. Chim. Acta*, 2017, **982**, 168–175.
145 X. Lu, L. Tao, D. Song, Y. Li and F. Gao, *Sensors Actuators, B Chem.*, 2018, **255**, 2575–2581.
146 H. Bai, M. Han, Y. Du, J. Bao and Z. Dai, *Chem. Commun.*, 2010, **46**, 1739–1741.
147 D. A. Gilbert, E. C. Burks, S. V. Ushakov, P. Abellan, I. Arslan, T. E. Felter, A. Navrotsky and K. Liu, *Chem. Mater.*, 2017, **29**, 9814–9818.
148 B. D. Adams, G. Wu, S. Nigro and A. Chen, *J. Am. Chem. Soc.*, 2009, **131**, 6930–6931.
149 Y. Lu, R. Jin and W. Chen, *Nanoscale*, 2011, **3**, 2476–2480.
150 T. Su, Z. L. Wang and Z. Wang, *Small*, 2019, **15**, 1900050.
151 E. A. Sutter and P. W. Sutter, *J. Am. Chem. Soc.*, 2014, **136**, 16865–16870.
152 D. Zhang, C. Jin, H. Tian, Y. Xiong, H. Zhang, P. Qiao, J. Fan, Z. Zhang, Z. Y. Li and J. Li, *Nanoscale*, 2017, **9**, 6327–6333.
153 F. Hayee, T. C. Narayan, N. Nadkarni, A. Baldi, A. L. Koh, M. Z. Bazant, R. Sinclair and J. A. Dionne, *Nat. Commun.*, 2018, **9**, 1775.
154 W. A. Saidi, H. Feng and K. A. Fichthorn, *J. Phys. Chem. C*, 2013, **117**, 1163–1171.
155 K. A. Fichthorn, T. Balankura and X. Qi, *CrystEngComm*, 2016, **18**, 5410–5417.
156 P. Y. Yang, S. P. Ju, Z. M. Lai, J. Sen Lin and J. Y. Hsieh, *Nanoscale*, 2016, **8**, 2041–2045.
157 S. P. Ju, M. H. Weng and W. C. Huang, *J. Mater. Chem.*, 2012, **22**, 20319–20333.
158 L. Y. Zhang, D. Wu, Y. Gong, H. Liu, W. Chen and L. Bi, *ChemElectroChem*, 2018, **5**, 2403–2408.
159 H. Peng, C. Rao, N. Zhang, X. Wang, W. Liu, W. Mao, L. Han, P. Zhang and S. Dai, *Angew. Chemie - Int. Ed.*, 2018, **57**, 8953–8957.
160 C. Peng, W. Yang, E. Wu, Y. Ma, Y. Zheng, Y. Nie, H. Zhang and J. Xu, *J. Alloys Compd.*, 2017, **698**, 250–258.
161 X. Chen, J. Wang, T. Odoom-Wubah, X. Jing, J. Huang, Q. Li and Y. Zheng, *Mater. Lett.*, 2016, **165**, 29–32.
162 Q. Tan, C. Du, Y. Sun, L. Du, G. Yin and Y. Gao, *Nanoscale*, 2015, **7**, 13656–13662.
163 D. Sun, L. Si, G. Fu, C. Liu, D. Sun, Y. Chen, Y. Tang and T. Lu, *J. Power Sources*, 2015, **280**, 141–146.
164 W. Hong, J. Wang and E. Wang, *Int. J. Hydrogen Energy*, 2014, **39**, 3226–3230.
165 C. Wang, L. Wang, R. Long, L. Ma, L. Wang, Z. Li and Y.

 

Xiong, *J. Mater. Chem.*, 2012, **22**, 8195–8198.
166 L. Hu, X. Cao, L. Shi, F. Qi, Z. Guo, J. Lu and H. Gu, *Org. Lett.*, 2011, **13**, 5640–5643.
167 W. Kang, H. Li, Y. Yan, P. Xiao, L. Zhu, K. Tang, Y. Zhu and Y. Qian, *J. Phys. Chem. C*, 2011, **115**, 6250–6256.
168 S. Wang, X. Wang and S. P. Jiang, *Nanotechnology*, 2008, **19**, 455602.
169 K. Naoe, C. Petit and M. P. Pileni, *Langmuir*, 2008, **24**, 2792–2798.
170 X. Teng, W. Q. Han, W. Ku and M. Hücker, *Angew. Chemie - Int. Ed.*, 2008, **47**, 2055–2058.
171 E. J. Menke, M. A. Thompson, C. Xiang, L. C. Yang and R. M. Penner, *Nat. Mater.*, 2006, **5**, 914–919.
172 C. H. Cui, J. W. Yu, H. H. Li, M. R. Gao, H. W. Liang and S. H. Yu, *ACS Nano*, 2011, **5**, 4211–4218.
173 Y. Zhang, M. Zhang, Z. Cai, M. Chen and F. Cheng, *Electrochim. Acta*, 2012, **68**, 172–177.
174 N. Tian, Z. Y. Zhou and S. G. Sun, *Chem. Commun.*, 2009, 1502–1504.

ARTICLE

**Table 2:** Summary of chemical methods for Pd-based NWs synthesis and their applications

| Compound | Structure | Synthesis approach | Surfactant/co-surfactants | Reducing agent | Reaction temperature and time | Solvent | Application | Ref. |
|---|---|---|---|---|---|---|---|---|
| **PdCu** | NCNs | Polyol | PVP/Pluronic F-127 | EG | 120/160/220 °C for 2 h each | EG | Formic acid oxidation | 108 |
| **PdIr** | NWs | Hydrothermal | Poly(diallyldimethylammonium chloride) solution | HCHO | 120 °C for 5 h | DI Water | Water splitting | 122 |
| **GaPd2** | NWs | Chemical reduction | Olalamine/Oleic Acid/ Trioctylphosphine | Hexamethyldisilazane (HMDS) | 320 °C for 100 min | 1-dodecanethiol | Hydrogen evolution reaction | 97 |
| **Pd** | NCNs | Chemical reduction | PVP/KBr | $NaBH_4$ | Room temp, N/A | DI Water | Oxygen reduction | 98 |
| **Pd@Au** | NRs | Soft-template | CTAB/Pluronics | AA | 43 °C for 25 min followed by 65 °C for 1 h | DI Water | Enhanced optical and LSPR properties | 93 |
| **PdAg** | NWs | Soft-template | Dioctadecyldimethylammonium chloride (DODAC) | AA | 95 °C for 2 h | DI Water | Ethanol oxidation | 11 |
| **PdCuP** | NWs | Soft-template | DODAC | $NAH_2PO_2$ | 95 °C for 2 h | DI Water | Ethanol oxidation | 88 |
| **Pd@Au** | NWs | Hydrothermal / bio-template | PVP/KI | PVP | 200 °C for 3 h | DI Water | Organophosphate pesticide detection | 99 |
| **PtPdCu** | NWs | Solvothermal | PVP/KBr | PVP/DMF | 200 °C for 4 h | DMF | Methanol and formic acid oxidation | 10 |
| **PdCu** | NWs | Solvothermal | PVP | EG/DMF | 170 °C for 8 h | EG/DMF | Ethylene glycol oxidation | 50 |
| **PdPt** | NWs | Soft-template | DODAC | AA | 95 °C for 30 min | DI Water | Hydrogen evolution | 64 |
| **AuPd** | NWNs | Chemical reduction | Theophylline | Hydrazine | Room temp for 1 min | DI Water | Formic acid oxidation | 80 |
| **PdRuPt** | NWNs | Chemical reduction | PVP/KBR | $NaBH_4$ | Room temp for 20 min | DI Water | Methanol electro-oxidation | 111 |
| **Pd** | NCNs | Chemical | Poly-l-lysine | Hydrazine | Room temp for 5 h | DI Water | Formic acid | 89 |

| | | | | | | | | |
|---|---|---|---|---|---|---|---|---|
| | | reduction | | | | | oxidation and hydrogen evolution reaction | |
| **PtPd** | NWs | Soft-template | CO | CO | Room temp for 4 h | DI Water | Oxygen reduction | 158 |
| **PdSn** | NCNs | Solvothermal | PVP/Citric Acid | EG | 220 °C for 10 h | EG | Formic acid oxidation | 106 |
| **PdCe** | NWs | Soft-template | NP-5 (polyethylene glycol mono-4-nonylphenyl ether) | Ammonia | Room temp for more than 48 h | Cyclohexane | Methane combustion | 159 |
| **Pd** | NWs | Hydrothermal | PVP/NaI | PVP | 200 °C for 2 h | DI Water | Optoelectronic trapping | 86 |
| **Pd** | NRs | Soft-template | CTAB/Pluronics | AA | 43 °C for 25 min followed by 65 °C for 1 h | DI Water | NA | 92 |
| **Pd@Au** | NRs | Hydrothermal | PVP | PVP | 200 °C for 4 hours | DI Water | Biosensor for OPs | 145 |
| **Pd** | NWs | Polyol | PVP/NAI | DEG | 160 °C for 1 h | DEG | Formic acid oxidation and Oxygen reduction | 44 |
| **Pd3Pb** | NWNs | Polyol | PVP | EG | 170 °C for 1 h | EG | Oxygen reduction and ethanol oxidation | 43 |
| **PdAu** | NWNs | Chemical reduction | PVP/KBr | NaBH4 | Room temp for 1 h | DMF/Benzyl alcohol/cyclohexane/DI Water | Oxidation of EG and isopropanol | 117 |
| **PdAg** | NTs | Polyol/ Galvanic Replacement | PVP | EG | 160 °C for 1 h | EG | Ethanol oxidation | 160 |
| **Pd** | NWNs | Chemical reduction | CTAB/Zn | $NaBH_4$ | 60 °C for 12 h | DI Water | Ethanol oxidation and hydrogen evolution reaction | 95 |
| **Pd** | NWs | Soft-template | DODAC | AA | 95 °C for 30 min before rapid injection | DI Water | Formic acid oxidation | 63 |
| **Au/Pd/Ag** | NWs | Soft-template (Bio template) | Pichia pastoris cells (PPCs) and CTAB | AA | 60 °C for 3 h | DI Water | NA | 161 |
| **PdIr** | NWNs | Hydrothermal | PVP/NAI | 2,7-Dihydroxynaphtha-lene (2,7-DHN) | 210 °C for 2 h | DI Water | Oxygen reduction | 49 |
| **PdAu** | NWs | Hydrothermal /Galvanic | PVP/NAI | PVP | 200 °C for 3 h | DI Water | Biosensor for OPs | 143 |
| **Pd** | NWs | Soft-template | CTAB/SDS/1-pentanol | Hydrogen | Room temp for 18 h | Brine/Toluene | Reduction of 4- | 66 |

| | | | | | | | | |
|---|---|---|---|---|---|---|---|---|
| | | (Liquid crystal) | | | | | nitrophenol to 4-aminophenol | |
| **PdAu,PtPd** | NCNs | Soft-template | 3-(N,N-Dimethylpalmitylammonio) propanesulfonate (PAPS) | $AA/NABH_4$ | 25 °C for 24 h | DI Water | Methanol oxidation reaction or formic acid oxidation | 62 |
| **PdPt** | NWNs | Chemical reduction | PVP/KBr | $NaBH_4$ | Room temp for 15 min | DI Water | Ethylene glycol & glycerol oxidation | 118 |
| **Pd** | NRs | Polyol | PVP/NaI | DEG | 160 °C for 1h | DEG | Template for bimetallic or hollow nanostructures | 54 |
| **PdCe** | NWNs | Solvothermal | None | EG | 170 °C for 2 h | EG | Ethanol/methanol oxiation | 162 |
| **PdCu; PdAu; PdPt** | NWNs | Chemical reduction | None/KCl | $NaBH_4$ | Room temp for 3 min | DI Water | Ethanol oxidation | 115 |
| **PdNi** | NWNs | Chemical reduction | trisodium citrate | $NaBH_4$ | Room temp for 2 h | DI Water | Formic acid oxidation | 110 |
| **PdCu, PtPdCu** | NWs | Soft-template | dodecyltrimethylammonium bromide (DTAB) | $NaBH_4$ | Room temp for 1 h | toluene/ octadecylamine | Small molecule oxidation | 107 |
| **PdIr** | NWNs | Hydrothermal | PVP/NaI | PVP/2,7-Dihydroxynaphthalene | 210 °C for 2 h | DI Water | Oxygen reduction | 48 |
| **PdSn** | NWNs | Solvothermal | None | EG | 180 °C for 2 h | EG | Formic acid oxidation | 163 |
| **Pd** | NWNs | Chemical reduction | PVP/KBr | $NaBH_4$ | Room temp for 30 min and stirring over night | DI Water | Formic acid oxidation | 164 |
| **PdBi** | NWs | Chemical reduction | Oleylamine | $NaBH_4$ | 90 °C for 30 min | Oleylamine | Formic acid and methanol oxidation | 96 |
| **Pd** | NRs | Chemical reduction | CTAB/KI | AA | 90 °C for 1-1.5 h | DI Water | Formic acid oxidation | 100 |
| **Pd** | NWs | Polyol synthesis | PVP | EG/DEG | 140 °C for 3 h | EG/DEG | Formic acid oxidation | 8 |
| **Pd-P** | NWNs | Soft-template | Polyethylene glycol hexadecyl ether | HCHO | 150 °C for 8 h | DI Water | Formic acid oxidation | 61 |
| **Pd** | NWNs | Soft-template | Octylphenoxy- polyethoxyethanol (OP-10) | $KBH_4$ | 0 (ice bath) for 5 min | DI Water | Formic acid oxidation | 105 |
| **PdAu** | NWNs | Chemical reduction | PVP/KBr | $NaBH_4$ | Room temp for 30 min | DI Water | Ethanol electrooxidation | 82 |
| **Pd, PdNi** | NWNs | Soft-template | Tetraoctylammonium bromide (TOAB) | $NaBH_4$ | Room temp for 24 h | Toluene | Hydrogenation of p-nitrophenol | 60 |

| | | | | | | | | |
|---|---|---|---|---|---|---|---|---|
| **PdNi** | NWs | Soft-template | ODA/DTAB | NABH4 | Room temp for 20 min | Toluene/Water | Oxygen reduction | 121 |
| **Pd** | NWs | Hydrothermal | PVP, NaI,CH3CN | HCHO | 140 °C for 4-12 h | DI Water | Reduction of 4-NP | 47 |
| **PdCu** | NWNs | Soft-template | Triton X-114 | NaBH4 | room temp for 30 min | DI Water | Ethanol oxidation | 114 |
| **PdPt** | NWs | Hydrothermal/Galvanic Replacement | PVP/NaI | PVP | 200 °C for 2 h | DI Water | Oxygen reduction | 120 |
| **PtPd** | NCNs | Chemical reduction | PVP | Hydrazine | Room temp for 1 h followed by stirring for 12 h | DI Water | Formic acid oxidation | 79 |
| **Pd** | NWs | Soft-template | CTAB/1-pentanol | Hydrazine hydrochloride | Room temp for 48 h | Toluene | NA | [59] |
| **Pd** | NWs | Hydrothermal | PVP/KI | PVP | 150 °C for 46 h | DI Water | Galvanic replacement | [165] |
| **PdAg** | NWs | Polyol | PVP | Ethylene glycol | 170 °C for 3 h | Ethylene glycol | Formic acid oxidation | [42] |
| **PdAu. PdPt** | NWs | Hard-template | None | $NaBH_4$ | Room temp for 30 min | Ethanol | Oxygen reduction | 119 |
| **Pd** | NWs | Soft-template | CTAB/dodecylamine | $NaBH_4$ | Room temp for 1 h | Toluene | Preparation of azo compounds from nitroaromatics | 166 |
| **Pd@carbon** | NWs | Hydrothermal | polyacrylamide/R-lactose monohydrate | AA | 200 °C for 6 h | DI Water | Ascorbic acid (AA) oxidation | 167 |
| **Pd** | NWNs | Chemical reduction | trisodium citrate | $KBH_4$ | room temp for 30 min | DI Water | Formic acid oxidation | 81 |
| **Pd** | NRs | Seed mediated, chemical reduction | CTAB | AA | 30 °C for 20 h | DI Water | Suzuki coupling | 53 |
| **Pd** | NWs | Soft-template | CTAB/Propanol | Electron beam irradiation | Room temp for few minutes | Cyclohexane/DI Water | Ethanol oxidation | 57 |
| **Pd** | NWs | Soft-template | PVP | Copper powder | 50 °C for 24 h | Methanol | Carbon–carbon cross-couplings | 58 |
| **Pd** | NWs | Hydrothermal | PVP/NaI | PVP | 200 °C for 2 h | DI Water | NA | 46 |
| **Pd** | NWNs | Chemical reduction | PSS | $NaBH_4$ | Room temp for 30 min | DI Water/ethanol | Direct formic acid fuel cells | 168 |

| | | | | | | | | |
|---|---|---|---|---|---|---|---|---|
| **Pd** | NWs | Soft-template | Sodium bis(2-ethylhexyl)-sulfosuccinate (AOT) | $NaBH_4$ | Room temp for 1 h | Isooctane/DI Water | NA | 169 |
| **Pd** | NWs | Soft-template | DTAB | $NaBH_4$ | Room temp for 80 min | octadecylamine (ODA) /toluene/DI Water | NA | 170 |
| **Pd** | NRs | Polyol | PVP/KBr | EG\PVP | 100 °C for 1 h | EG | NA | 38 |
| **Pd** | NWs | Seed mediated-Chemical reduction | 1-methyl-3-(2'-mercaptoacetoxyethyl) imidazolium chloride (TFIL) | $NaBH_4$ | Room temp, N/A | TFIL | Sonogashira coupling | 55 |

We review the synthesis, characterization, and applications of one-dimensional palladium-based nanostructures and provide perspective on future directions in this field.